Chem Soc Rev

A tutorial on the modeling of the heterogenous captured CO2 electroreduction reaction and first principles electrochemical modeling

Journal:	*Chemical Society Reviews*
Manuscript ID	CS-REV-12-2024-001210.R1
Article Type:	Tutorial Review
Date Submitted by the Author:	16-Apr-2025
Complete List of Authors:	Kowalski, Robert; University of California Los Angeles Cheng, Dongfang; University of California Los Angeles Sautet, Philippe; University of California Los Angeles,

A tutorial on the modeling of the heterogenous captured CO_2 electroreduction reaction and first principles electrochemical modeling

Robert Michael Kowalski, Dongfang Cheng, and Philippe Sautet*

Five Learning Objectives

1. **Motivation behind captured CO_2 reduction reaction(c-CO_2RR) as compared to CO_2 reduction reaction(CO_2RR)**
2. **Reaction mechanism of the electroreduction of the captured CO_2**
3. **Accounting for the potential and pH in the modelling of c-CO_2RR and other electrochemical reactions**
4. **Modeling techniques typically used in modeling the c-CO_2RR and electrochemical reactions as a whole**
5. **Techniques used to modeling the reactivity of the c-CO_2RR, CO_2RR, and HER**

Abstract

As the energy demands of the world continues to grow, the electroreduction of captured CO_2 (c-CO_2RR) is an appealing alternative to the traditional CO_2 reduction reaction (CO_2RR) as it does not include the energetically unfavorable release of CO_2 from the capture agent. In this tutorial we cover the motivation behind the c-CO_2RR and CO_2RR, their respective mechanisms, and computational tools that have been used to model these reactions and to compare their reactivities. Emphasis is given to methods that have already been used to model the c-CO_2RR but a comparison to the methods used to explore the more understood CO_2RR are covered as well.

1. Motivation behind captured CO_2 reduction reaction(c-CO_2RR) as compared to CO_2 reduction reaction (CO_2RR)

1.1 Motivation for Converting CO_2

Over the past 100 years the concentration of atmospheric CO_2 has drastically increased.[1] This has caused various issues such as rising average surface temperatures and changes in ocean pH, both of which wreak havoc on the natural ecosystem.[2,3]

This large increase in CO_2 concentration mainly comes from our society's dependence on burning fossil fuels for energy. CO_2 is the majority byproduct of the consumption of fossil fuels, and in 2017 it was estimated that more than 30 Gtonnes of CO_2 enter the atmosphere annually.[4] More recently, in 2023 the yearly CO_2 emission we about 35 Gtonnes per year and the atmospheric concentration of CO_2 was 420 ppm.[5] Therefore, significant work has been conducted on exploring mitigation methods. A leading approach is carbon capture and utilization (CCU).[6] In this method, the carbon is converted into higher values products such as fuels, chemicals, and concrete, leading to a more sustainable cycle.[7–11] This tutorial begins with an explanation on the CO_2 reduction

reaction and challenges it presents. We present an alternative, the captured CO_2 reduction reaction (c-CO_2RR). We then explore the various reaction pathways that have been studied for the CO_2RR and the c-CO_2RR. We include a brief overview of various solvation methods and of calculations including the effect of potential. We finish this tutorial by explaining some of the current methods to measure the activity of the c-CO_2RR as well as challenges that have been identified. We hope this tutorial will give the reader insight into how to run calculations on the CO_2RR and c-CO_2RR and what are the current gaps in the literature. We also hope that this tutorial will provide information on solvation methods and calculations under the influence of potential that can be used for calculations beyond CO_2 conversion.

1.2 CO_2 Reduction Reaction (CO_2RR) background

One of the proposed solutions under CCU is the CO_2 reduction reaction (CO_2RR). This process can be done electrochemically or thermochemically, but this review will focus on the electrochemical reduction of CO_2 and captured CO_2.[12–16] In the CO_2RR, the CO_2 is directly reduced into a variety of products depending on the catalyst used. For example, literature has shown that metals such as Ag and Au have a high selectivity for CO,[17,18] while metals such as Sn and In show high selectivity for formic acid.[19,20] Of the metals, Cu is the only know catalyst to be able to directly reduce CO_2 into methane and multi-carbon products, like ethylene and ethanol.[21]

1.2.1 Implementation

However, implementing the CO_2RR industrially is challenging. To produce reasonable currents, it is first necessary to capture and concentrate the CO_2.[22] Traditionally, amines have been used as CO_2 sorbents, with the most common amine being monoethanol amine (MEA).[23] Figure 1 plots the thermodynamic profile for the capture of CO_2 using MEA.

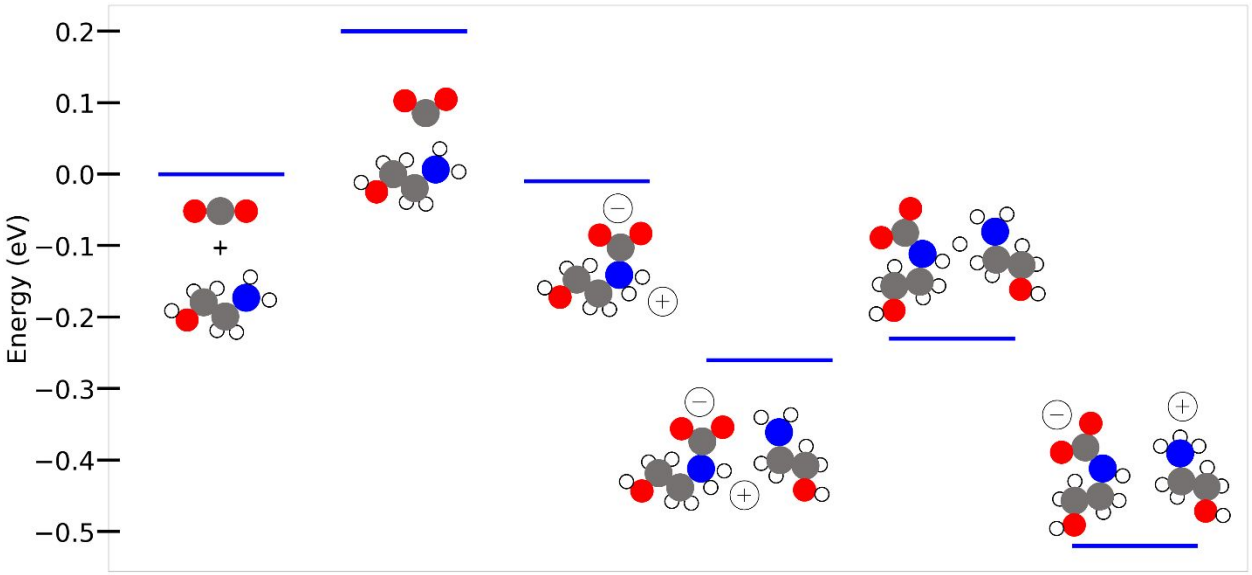

Figure 1: Reaction pathway of the capture of CO_2 by monoethanol amine (MEA). The + refers to a positively charge molecule and the – referes to a negatively charge molecule. The functional was B3LYP using an implict water solvent using Gaussian 09. Adapted from: [24]

It is to be observed that two MEA are required to capture one CO_2. A first MEA moleucle interacts with a CO_2 molecule to form a zwitterion in an thermodynamically neutral process. However, this zwitterion quickly reacts with another MEA to form a ammonium carbamate. This process is exergonic and the overall change in free energy is -0.52 eV.[24]

Therefore, as a capture agent, MEA performs well. However, in the context of reducing the CO_2 this is only half of the battle. After the carbamate has been formed it is then concentrated. Then energy is used to release the CO_2 from the carbamate complex, reforming the MEA and leaving concentraed free CO_2. However, this process is highly energy intensive.

It is to be noted that the adsorption of CO_2 is known to be pressure dependent. Previous work by Arstad *et al*. showed that by increaseing the partial pressure of CO_2 from 1 atm to 25 atm, the adsorption of CO_2 onto amine functionalized metal organic frameworks (MOFs) could be improved from 14 wt% to 60 wt%.[25] Another study by Afkhamipour *et al*. explored the equiibrium constants for CO_2 adsoprtion using amines in adsorption towers.[26] They found that the flux of CO_2 is dependent on the difference in CO_2 partial pressure between the bulk and the interface. Additionally, they found that the equilibrium constant for CO_2 adsorption is dependent on the system pressure.[26]

Therefore, it has been propsed to reduce the captured CO_2 (c-CO_2RR) instead of having to first capture and release the CO_2. Since CO_2 is stabilisized in the complex with the capture agent, the electroreduction of captured CO_2 (c-CO_2RR) is more difficult than the electroreduuction of free CO_2. Therefore, challenges present in the CO_2RR will be bigger challenges in the c-CO_2RR as well as other challenges that occur from introducing the negavtively charged captured CO_2 near the cathode. Therefore, a key question is to determine what sorbent should be used to provide the best chance for c-CO_2RR.

Although not explicititly about the c-CO_2RR, Appel *et al*. proposed that weaker bond require lower overpotential to break.[27] Zhang *et al*. explored three types of CO_2 sorbents: amines, alkoxides, and phenoxides. In their work they used the term pK_{CO2} which was based on the CO_2 binding free energy from an anionic capture agent to form the anioic captured CO_2. Figure 2 displays the typical range of CO_2 binding free energies that they determined as well as a cartoon of the reaction they considered.[28]

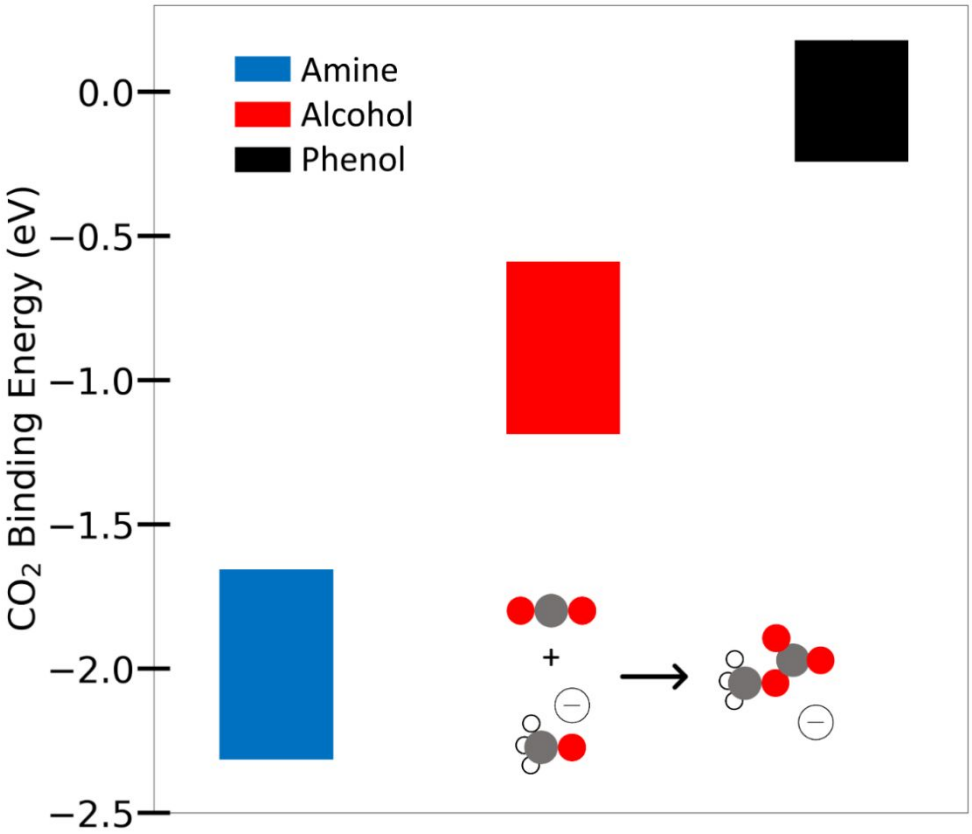

Figure 2: The typical range of CO_2 binding energies to the deprotonated capture agent (in an anionic form). Various amines, alcohols, and phenols were screened. The picture at the bottom shows a cartoon of the reaction considered when methanol is the capture agent. Calculations were conducted in Gaussian 16, using the B3LYP-D3 functional and an implicit solvent. Adapted from: [28]

From Figure 2 it becomes clear that for pure CO_2 capture, amines are the best of the three proposed families of capture agents, as they bind CO_2 the strongest. Likewise, phenoxides are the worst as pure capture agents, as they provide the weakest binding. However, this also means that breaking the bond between the CO_2 and the amine will be the most endergonic, while breaking the bond between the CO_2 and the phenoxide will be the least endergonic. Given that the goal of the capture agent is to concentrate the CO_2 so that the CO_2RR can have reasonable currents, using amines will incur the largest energy penalty, of the three capture agent families, when the CO_2 is released from the capture agent.

However, as stated it is proposed to bypass this decomposition by directly reducing the capture agent. Using Appel *et al.*'s conclusion it can be predicted that the overpotentials required for the direct reduction of alkoxide captured CO_2 should be smaller than that for amine captured CO_2, and the overpotentials for the direct reduction of phenoxide captured CO_2 should be even smaller.

To our knowledge most of the literature has focused on the direct reduction of amine captured CO_2 and of bicarbonate (H_2O captured CO_2).[29–33] These are common starting points as

amines are the most common industrial capture agent, and (bi)carbonate ions are present in any CO_2RR reaction network through the various equilibriums between CO_2 and H_2O.[34] However, there is very little research on alkoxide c-CO_2RR[31] and to our knowledge no published literature on phenoxide c-CO_2RR. Thus, more work must be completed on exploring the effect of the capture agent on the c-CO_2RR.

It is important to note the large differences between the CO_2 binding energies reported by Darvan-Candan *et al*. and Zhang *et al.,* as these discrepancies stem from their distinct methodological approaches. Darvan-Candan *et al*. presented a detailed reaction pathway which considers the overall neutrality of the reactants and products, ensuring a balanced charge state throughout the reaction process.[24] However, Zhang *et al*. conducted a broad screening study, aiming to evaluate trends between the different types of capture agents. For simplicity, they evaluated the capture agent in its anionic form.[28] Notably, what Zhang *et al*. provides is a motivation to search for other capture agents past the typical amines.

Although, the capture and concentration processes are typically not considered in works exploring the CO_2RR, the goal of this section was to motivate the reader to consider that aspect of the CO_2RR as well. Figure 3 provides a cartoon of the full CO_2RR process as well as the alternative c-CO_2RR pathway.

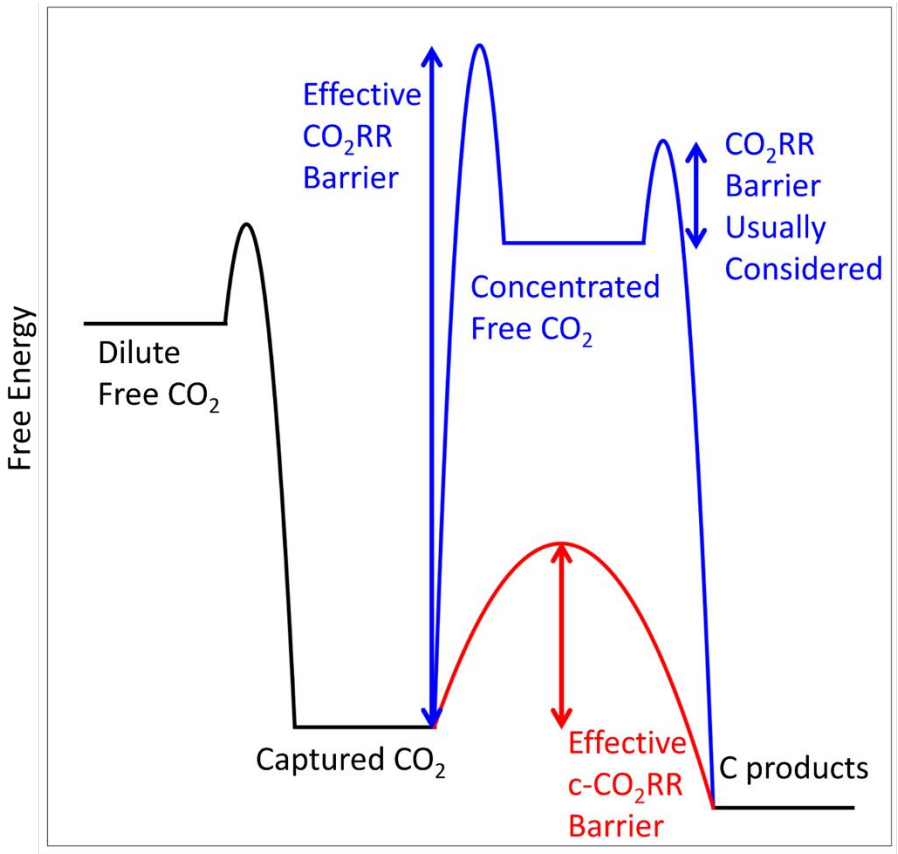

Figure 3: Cartoon depicting the thermodynamic question to be answered by researching the c-CO_2RR. Is it possible to find a c-CO_2RR system such that the effective barrier of the c-CO_2RR is smaller than the CO_2RR?

Typically, papers that explore the CO_2RR start with concentrated free CO_2 and reduce that to various products. Therefore, the effective barriers typically shown in these works is labeled as "CO_2RR Barrier Usually Considered" in Figure 3. However, what is not considered is the energy to concentrate this CO_2. Starting from dilute CO_2 the overall thermodynamics between dilute CO_2 and the product CO is identical regardless of if the CO_2 is captured and released before the reduction or of the captured CO_2 complex is directly reduced. Given that the capture process is exergonic, it is clear decomposing the complex will be endergonic. When this decomposition is added to the CO_2RR a significant thermodynamic barrier appears in the CO_2RR pathway. In Figure 3 this is labeled as "Effective CO_2RR Barrier". However, once passed the CO_2RR can conduct as it is typically presented. Concentrating the CO_2 decreases the entropy, this leads to a less stable concentrated free CO_2 than dilute free CO_2. From this point the traditional CO_2RR occurs. From this point we refer to the full CO_2RR as the mechanism including the CO_2 capture and release as part of the CO_2RR mechanism (Figure 3).

What is less understood is the relationship between the effective CO_2RR barrier of the full CO_2RR and the effective c-CO_2RR barrier Previous work has shown that with a strong enough proton source, the intrinsic thermodynamics of the c-CO_2RR is more favorable than the CO_2RR.[31] Therefore, it has been proposed to directly reduce the captured CO_2 as compared to having to first release the CO_2 from the capture agent. However, the success of c-CO_2RR will critically depend on the potential dependent energy profile and kinetic barriers.

2. Reaction mechanism of the electroreduction of the captured CO_2

In the c-CO_2RR reaction network, there are three reactions possible: the c-CO_2RR, the typical CO_2RR (from any free CO_2 dissolved in the solvent), and the competing hydrogen evolution reaction (HER).[31]

2.1 Various CO_2RR mechanisms

It is to be noted that for all of the mechanisms and products considered CO_2 will need to adsorb to the surface at some point. Various literatures have shown the importance of the presence of cations to improve the CO_2 binding.[35,36] Cations also provide some charge to the electrode as seen by the electrolyte effect on the potential of zero charge.[37,38] In the gas phase CO_2 is a linear molecule. However, when CO_2 bind to an electrocatalyst surface, it is predicted that it binds in a bent conformation. The binding of CO_2 has been shown to be stabilized by the presence of cations and hydrogen bonding from the surface[39–41] It should be noted that not all cations improve the CO_2RR reactivity in the same way. It has been found that increasing the size of the cation can lead to better reactivity for CO_2RR.[39,42] For the c-CO_2RR most current literature has proposed K as the cation,[31,33] but further work remains on determining the cation effect in the c-CO_2RR.

2.1.1 CO and Formic Acid Production

In the context of c-CO_2RR, the only products that have been extensively studied are CO formic acid, and methane. Thus, this review will mainly focus on their production. Equations 1 and 2 show the overall balanced reaction to convert CO_2 into CO and formic acid, respectively.[43]

$$CO_2 + 2(H^+ + e^-) \rightarrow CO + H_2O \quad (1)$$

$$CO_2 + 2(H^+ + e^-) \rightarrow HCOOH \quad (2)$$

Free CO_2 first binds to the surface through a partial decoupled electron transfer and then is protonated to form COOH*,[44] although the nature of this adsorption and protonation as well as the amount of charge transferred in each step has been debated.[45,46] This effect is observed by a potential dependence on the CO_2 adsorption.[31] It has been shown that the presence of cations assists the adsorption of CO_2 by providing lateral electrons to stabilize the bent CO_2.[35] Additionally, the cation will be present near the surface as it is part of the electric double layer. Therefore, to properly model the active site it is advisable to include an explicit cation in calculation.

However, most density function theory (DFT) calculations on the CO_2 do not include an explicit cation.[47,48] Typically, properly solvating the cation involves expensive *ab-initio* molecular dynamics (AIMD),[49,50] which is unreasonable to conduct for each reaction intermediate. Additionally, many papers use the computational hydrogen electrode model (Section 3.1) because it allows for simple analysis of the electrochemical steps.[51–54] A drawback, however, is that it cannot decouple proton and electron transfers, and as such the decoupled proton-electron transfer between the gas-phase CO_2 and the COOH* cannot be properly modelled. Note that COOH* will undergo one PCET process to form *CO and H_2O, in a surface-assisted bond cleavage. Finally, CO desorbs to complete the cycle.[55]

It has been found that formic acid is typically the major product on some post transition metals such as In, Sn, Pb, and Bi, and materials derived from these elements.[56–71] Similar to the CO_2RR, the formic acid pathway contains two PCETs. However, unlike the CO production pathway where the COOH* is the product of CO_2 undergoing a PCET, OCHO* is produced. This OCHO* will undergo a final PCET to produce formic acid. Some works include a specific formic acid desorption step while others assume that the desorption is coupled with the final PCET.[58,66] Previous work has used COOH* binding as a descriptor for CO production and OCHO* binding as a descriptor for formic acid production.[60]

It has also been proposed that on catalysts that have an affinity for H adsorption, the surface H could be the proton source for the formate generation in an uncoupled proton electron transfer. Importantly, this mechanism has even been shown to occur on Ag,[48] a metal that under the right conditions has achieved high faradaic efficiencies for CO and poor affinity for H adsorption.[17,72–74] It has been shown that the presence of the formate greatly weakens the H binding energy, while only slightly weaking the COOH* binding energy. Thus, it has been proposed that the presence of formate improves the selectivity to CO by hindering the HER pathway.[48] However, what is less understood is relationship between the selectivity for formic acid and CO on Ag.

It is important to understand how these metals conduct the c-CO_2RR. There is not an intrinsic reason that metals that produce certain products during the CO_2RR must produce the same products during the c-CO_2RR, as the c-CO_2RR mechanism is different than the CO_2RR (Section 2.2). However, these pathways remain poorly understood. Cu is the only known metal that forms products other than CO and formic acid.[12] Therefore, much literature has been focused on the CO_2RR on Cu and Cu-based catalysts.[12,75–77] However, challenges remain with using Cu in the c-CO_2RR. In the case of carbamate reduction, the carbamate is an anion. Thus, to bring the carbamate to the cathode, it is accompanied by a cation. Figure 1 showed that the production of carbamate always leads to an ammonium cation which are in equilibrium with amines. However, it has been shown that amines can corrode copper electrodes,[78] and therefore, no significant results have been reported using Cu to reduce amine-captured CO_2.[79] However, as Cu is the only known metal to be able to produce reduction products other than CO and formic acid, further work is needed to explore Cu as a catalyst for the c-CO_2RR. For completeness a brief explanation of the CO_2RR mechanism on Cu follows.

2.1.2 C_1, C_2, and C_2^+ products

Several decades ago, Hori *et al.* systematically studied various metal catalysts for CO_2 electroreduction and categorized them into four distinct groups based on their primary products: Au, Ag, Zn, Pd, and Ga predominantly produce CO; Pb, Hg, In, Sn, and Bi generate formate; Ni, Fe, Pt, and Ti mainly catalyze hydrogen evolution (H_2); while Cu uniquely yields substantial amounts of multi-carbon (C_2+) products.[80,81] Bagger *et al.* further attributed this unique capability of Cu to its distinctive adsorption characteristics—Cu being the only metal exhibiting a negative adsorption energy for *CO coupled with positive adsorption energy for *H.[82] To date, Cu remains the most effective electrocatalyst among transition metals for selectively converting CO_2 into valuable multi-carbon products, such as ethylene and ethanol. This exceptional selectivity arises from Cu's moderate and balanced adsorption strengths toward critical intermediates (*CO and *H), enabling efficient protonation and carbon-carbon coupling reactions, rather than producing single-carbon or hydrogen products.

However, caution must be exercised when extrapolating insights from conventional CO_2RR to c-CO_2RR, as the reaction environments and pathways differ significantly. Although Cu is highly effective at converting CO to multi-carbon products in traditional electrochemical settings, its capability to catalyze captured CO_2 directly to CO remains uncertain. Indeed, the underlying mechanism for CO_2-to-CO differs substantially in c-CO_2RR compared to standard aqueous-phase CO_2RR, and no studies to date conclusively demonstrate efficient CO_2-to-CO conversion by pure Cu under c-CO_2RR conditions. Consequently, it remains doubtful that a pure Cu catalyst can drive c-CO_2RR to multi-carbon products. A promising alternative could be the design of tandem catalysts combining Cu with Ag, where Ag effectively converts captured CO_2 to CO, which then spills over to Cu sites for subsequent protonation and C–C coupling.

2.1.2.1 Methane production

The other main C_1 product besides CO and formic acid is methane. The overall reaction is shown as equation 3.

$$CO_2 + 8(H^+ + e^-) \rightarrow CH_4 + 2H_2O \quad (3)$$

Following the two PCETs to convert CO_2 into CO, six other PCETs are necessary to produce methane. The first is to protonate the CO into HCO* through a third PCET. Three more PCETs occur to remove a H_2O and leave CH_2* onto the surface. The cycle is completed by 2 final PCETs to produce methane which desorbs from the surface.[83] Traditionally, methane is produced on Cu,[84,85] but Cu is typically known for its C_2 products.[86–88]

2.1.2.2 C-C coupling

C-C Coupling is known as the crucial elementary step on Cu since this step is the key for generating multi-carbon products. While there are various proposed mechanisms for this process, strong evidence points to C-C coupling as a rate-determining step (RDS) that does not involve proton transfer, which behaves as pH-independent.[12] Vibrational spectra and kinetic models have identified CO as the primary intermediate on Cu under reduction conditions, making the dimerization of 2 CO to form the *COCO intermediate the most widely accepted mechanism for C-C coupling on the surface.[89] Following C-C coupling, *COCO can be further transformed into the *COCOH intermediate, as directly observed by in situ Fourier-transform infrared spectroscopy (FTIR).[90] Initially, Hori and colleagues suggested that dimerization of two *CH_2 groups or the insertion of *CO to form *CH_2CHO were the main pathways for C-C coupling.[91] These processes were considered favorable from a thermodynamic and kinetic standpoint.[92] However, the energetics of CO protonation to *COH or *CHO present substantial barriers,[93] which contradicts experimental findings that the activity for C_2^+ products depend on the absolute potential.

Challenging this view, Xu *et al*. demonstrated that the reaction orders of adsorbed CO change from first to zero order as the partial pressure of CO shifts from less than 0.4 atm to more than 0.6 atm, suggesting that C-C coupling might not be the RDS in the formation of C_2^+ products in CO_2 reduction.[94] They proposed that instead, the hydrogenation of CO with adsorbed water could be the RDS. However, recent contributions by Seger and Gong *et al*. have critiqued this interpretation.[95] By applying an interval linear fit to kinetic data, they argue that this analysis could lead to incorrect conclusions about the CO reaction order varying between 1 and 0 with CO pressure changes. Their reevaluation supports the idea that the coupling of two adsorbed *CO molecules remains the RDS for creating multi-carbon products.

Initial calculations performed in vacuum conditions suggested that the energy barriers for CO-CO coupling on copper surfaces, including terrace (111), (100), and step (211) facets, were prohibitively high.[92] These early studies, however, did not fully account for the complexities of

the electrochemical interface, notably omitting factors like the solvent environment and the electrical field, both of which can significantly influence reaction energies by stabilizing C_2 intermediates that have large dipole moments. Nørskov *et al*. demonstrated a pivotal shift in understanding C-C coupling by incorporating the effects of a charged electrolyte into their models via one layer of charged water with either hydronium ion or explicit cation.[96] Their findings revealed that, under electrochemical conditions, the barriers for CO dimerization on the (111) and (100) facets of copper could be dramatically reduced to 0.68 eV and 0.33 eV, respectively. This reduction, particularly a 0.3 eV decrease over the (100) facet, implies an increase in the turnover frequency (TOF) by at least five orders of magnitude. This aligns with experimental evidence showing that C-C coupling occurs preferentially on the Cu (100) facet. With the C-C coupling barrier now deemed surmountable, attention has turned to subsequent steps, such as the surface hydrogenation of the *COCO intermediate, as potential rate-determining factors. Liu *et al*. explored this further by conducting microkinetic modelling, they found that at low overpotentials, the pathway involving *COCOH dominates, with the formation of C_2^+ products being limited by the protonation of *COCO. They reported a Tafel slope of 119 mV/dec for reactions following this pathway, closely matching experimental observations, which show a slope of 116 mV/dec.[89] Peng and co-authors emphasized the role of surface atom *C. Their studies suggest that while the OCCOH pathway may be prevalent in the early stages of reduction, at more negative potentials (below −0.5 V vs. RHE), the coupling of surface *C with CO emerges as the dominant route for generating C_2 products.[97]

Bell and Head-Gordon *et al*. discovered that the form of C-C coupling during the electrochemical reduction of CO_2 on copper surfaces varies with the applied electrical potential via grand canonical DFT calculations.[98] At lower overpotentials, the dimerization of two surface-bound *CO molecules is favored, presenting a reaction barrier of 0.53 eV at 0V versus the reversible hydrogen electrode (RHE). However, at higher overpotentials, the coupling of *CO with an adsorbed *CHO becomes the more favorable route. Goddard *et al*. employed ab initio molecular meta-dynamics simulations (AIMμD) alongside a model incorporating five layers of explicit water molecules.[99,100] Their findings suggest that the free energy barrier for CO-CO coupling on Cu (100) is 0.69 eV when the applied potential is less negative than -0.6V versus RHE. Following this coupling step, *COCO is rapidly protonated to *COCOH and then to *COHCOH, with each step involving relatively low reaction barriers. Notably, these steps proceed via the Eley-Rideal (ER) mechanism, where the proton source is H_2O, rather than adsorbed hydrogen (*H) on the surface. These insights underscore the significant impact of the solution environment and the electric field at the electrochemical interface on the behavior of C_2 intermediates. The variability in outcomes from different theoretical approaches to modeling this interface highlights the need for further methodological development in ab initio simulations of the electrochemical interface. By refining

these methods and establishing more accurate kinetic models, researchers can gain a deeper understanding of the trends in CO_2 reduction to C_2^+ products.

C-C coupling is not only a process influenced by the applied potential and the electrochemical environment but is also significantly dependent on the structural characteristics of the catalyst surface. Historically, Hori *et al.* demonstrated that Cu(111) tends to favor CH_4 production, while Cu(100) produces more C_2+ products, such as C_2H_4.[80,101] Further refining this notion, introducing step edges on Cu(100) facets, for instance, on Cu(711) or Cu(510), substantially increases the formation of C_2 species, whereas Cu(110) and Cu(210) still predominantly yield CH_4. Jaramillo *et al.* synthesized a Cu(751) surface rich in undercoordinated sites and observed an increased yield of oxygenated products, further work attribute this to the ability of low-coordination sites to stabilize intermediates like $*CH_2CHO$.[102,103] These results highlight the critical role of step edges and kinks in facilitating multi-carbon and oxygenated product formation.[98,99] In addition, the presence of square motifs on these surfaces has been highlighted as critical for facilitating this process.[103,104] Despite these insights, the structural sensitivity of Cu remains a matter of debate. Single-crystal electrodes are often prepared by electropolishing or mechanical polishing, which introduces numerous defects and means the "single crystal" surfaces tested in electrochemical cells are not truly pristine. Roldan *et al.* revisited facet-dependent activity on ultraclean single-crystal Cu electrodes prepared in ultrahigh vacuum (UHV). They found that genuinely clean Cu(111) and Cu(100) are, in fact, nearly inactive for CO_2RR, and hydrocarbon products appear only when defects are introduced.[105] Our recent work explains this phenomenon and reshapes the structure–activity relationship: the sluggish CO_2 activation and unfavorable CO binding on pristine Cu(111) and Cu(100) make these planar surface inert in CO_2RR, and strong CO adsorption on step and kink sites drives surface restructuring under reaction conditions. As defects proliferate, hydrocarbon formation becomes feasible. Moreover, while CH_4 tends to dominate when defects form on Cu(111) planar, Cu(100)-like terraces yield more C_2H_4, indicating that square motifs near step edges are key for C–C coupling.[106]

2.1.2.3 Bifurcation pathway for C_2H_4 and C_2H_5OH

The selectivity towards ethylene (C_2H_4) and ethanol (C_2H_5OH) during the electrochemical reduction of CO_2 on copper surfaces is a critical area of research due to its implications for the production of specific valuable chemicals. Understanding the pathways that lead to these products is essential for optimizing catalyst performance. Koper and colleagues have made significant strides in identifying the bifurcation pathways that determine the selectivity for these two products. Their thermodynamic analyses suggest that $*CH_2CHO$ is a critical intermediate that determines the selectivity between C_2H_4 and C_2H_5OH.[107] The fate of $*CH_2CHO$ can diverge in two directions:

if the C-O bond breaks, C_2H_4 is produced along with the release of an oxygen atom on the surface; alternatively, continuous protonation of *CH_2CHO leads to the formation of C_2H_5OH. This proposed pathway has been successful in explaining various experimental observations, such as the higher selectivity towards C_2H_4 over C_2H_5OH on Cu(100) surfaces,[108] the increased production of alcohols on surfaces with copper vacancies,[109] and the identification of active sites on OD-Cu catalysts.[103] Very recent work by Wu, Senftle, and colleagues proved that *O binding energy could be an efficient descriptor for determining whether breaking the C-O bond or not.[110] Gong *et al* . used the same descriptor and above mentioned pathway to screen the catalyst with high selectivity for ethylene and ethanol, and successfully explains the high performance seen on CuAl catalyst.[111] Based on those combined theory and experiments works, this pathway is widely regarded as the most likely mechanism for the differentiation between C_2H_4 and C_2H_5OH production.

Hori and colleagues have shown that acetaldehyde can be easily reduced to C_2H_5OH, highlighting the role of aldehydes as intermediates in the pathway to alcohols.[91] Their findings reveal that aldehyde formation occurs at lower overpotentials compared to alcohols; however, as the overpotential increases, alcohol production becomes more dominant. This observation was further supported by direct evidence from Chorkendorff and his team,[112] who observed acetaldehyde as an intermediate during the CO_2 electroreduction to C_2H_5OH on OD-Cu catalysts.

The intriguing observation that C_2H_5OH produced during CO_2 reduction in H_2O^{18} solution predominantly contains O^{18} molecules led researchers to speculate about the role of water in the CO_2RR. This finding implies that water might be directly involved in the formation of certain products. In response to these experimental results, Goddard *et al*. explored an alternative mechanism for the pathways leading to C_2H_4 and alcohols. Utilizing quantum mechanics (QM)-based meta-dynamic calculations, they discovered a pathway wherein a chain of six water molecules react with a *C-CH intermediate to form *CH-CHOH, which then undergoes further protonation to become C_2H_5OH. According to this model, ethylene is produced through the continuous hydrogenation of *C-CH, making *CCH the selectivity-determining intermediate instead of *CH_2CHO.[113] However, A. T. Bell *et al.* have proposed a different interpretation. They suggested that the integration of O^{18} into C_2H_5OH may result from isotopic scrambling between a carbonyl-containing intermediate and solvent water, a hypothesis supported by both experimental and theoretical studies. This interpretation advises caution in concluding that water is the direct source of oxygen in C_2H_5OH. Moreover, Bell and Head-Gordon have introduced another perspective on the bifurcation pathway for C_2H_4 and C_2H_5OH formation, based on an implicit electrolyte model with a fixed electrode potential. They identified *COCHO as a pivotal intermediate, with its protonation to *COCHOH at low overpotentials leading to C_2H_4 production. At higher overpotentials, they suggest that glyoxal (OCHCHO) formation followed by its reduction to acetaldehyde and subsequently to C_2H_5OH is the preferred pathway.[114]

There is currently no consensus on the definitive bifurcation pathway for C_2H_4 and C_2H_5OH production. The field necessitates further research, focusing on the kinetics of each step in the C_2 pathway within an accurate electrochemical interface model, rather than solely on thermodynamic considerations. Crucially, the ongoing refinement of density functional theory (DFT) models should be informed by experimental feedback to enhance the accuracy and predictive power of these theoretical frameworks.[115] This iterative process between experimental observations and theoretical modeling is essential for advancing our understanding of CO_2RR mechanisms and improving the selectivity and efficiency of catalysts for desired products.

2.2 Currently Explored Generalized c-CO_2RR Mechanisms

Most of the work on the c-CO_2RR to this point has focused on the formation of CO. As this process combines the reduction of CO_2 (requiring 2 protonations) and the release of the CO_2 from the capture agent (1 protonation) there are 3 required protonations per c-CO_2RR cycle. However, as equation 4 shows there are only 2 available electrons per reaction cycle.[31]

$$KRCO_2 + 3XH + 2e^- \rightarrow CO\,H_2O + 2X^- + RH + KX \quad (4)$$

In equation 4, RH refers to a generalized capture agent, XH is a generalized proton source, and KX is the resultant salt. Figure 4 provides a cartoon that explains the overall c-CO_2RR reaction via a worked example using potassium carbamate reduction and water as the proton source, while Figure 5 shows a cartoon of the elementary mechanism. In Figure 4, the capture agent RH is NH_3 (shown in red), the proton source XH is H_2O (shown in blue), and the resultant salt KX is KOH (shown in green).

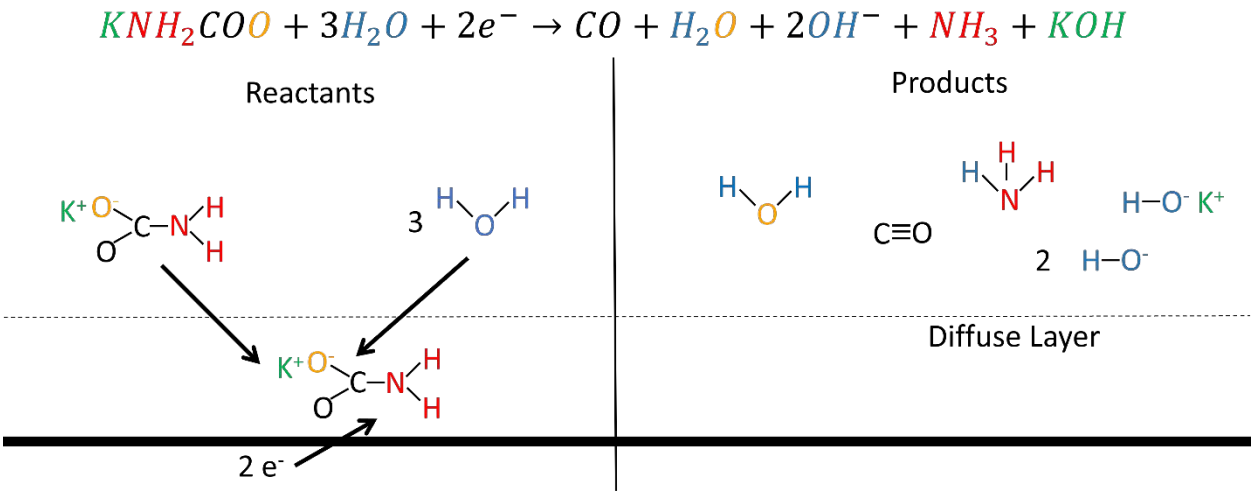

Figure 4: A worked example of the overall carbamate reduction using a water proton source. Color coding is provided to aid the reader in determining how the atoms rearrange. The capture agent RH (NH_3) is shown in red, the proton source XH (H_2O) is shown in blue and the resultant salt KX (KOH) is shown in green. The O of the carbamate are coded orange and black to shown that the

two O end up on different products (CO and H_2O) in the final product. In this case R is NH_2, and X is OH.

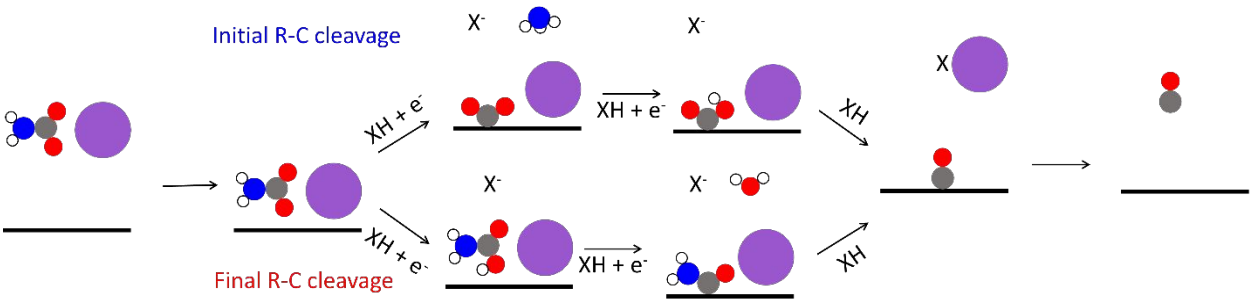

Figure 5: Most thermodynamically favorable pathways determined for the c-CO_2RR. In this case the capture agent RH is NH_3. XH refers to a generalized proton source. The corresponding structures are shown in Table 1. Adapted from: [31]

Table 1: Structures used in previous work that corresponds to the cartoon pathway in Figure 5. For the salt we assume the proton source was H_2O, so the salt is KOH. This can be changed for whichever proton source was used.

Cartoon	Part on Surface	Part in Solution
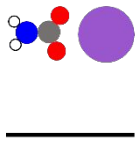	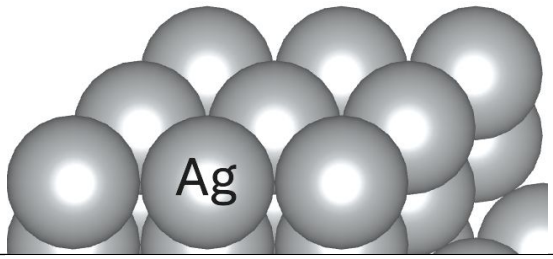	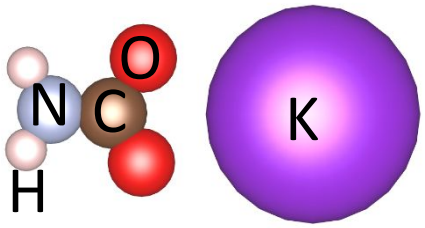
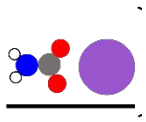	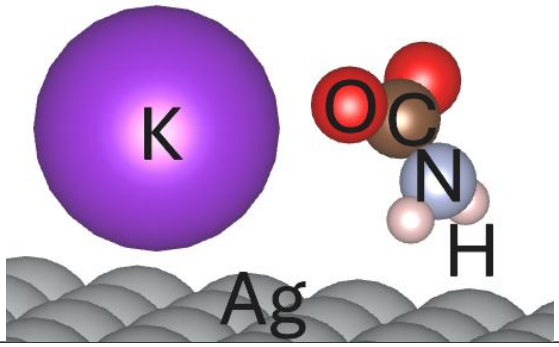	

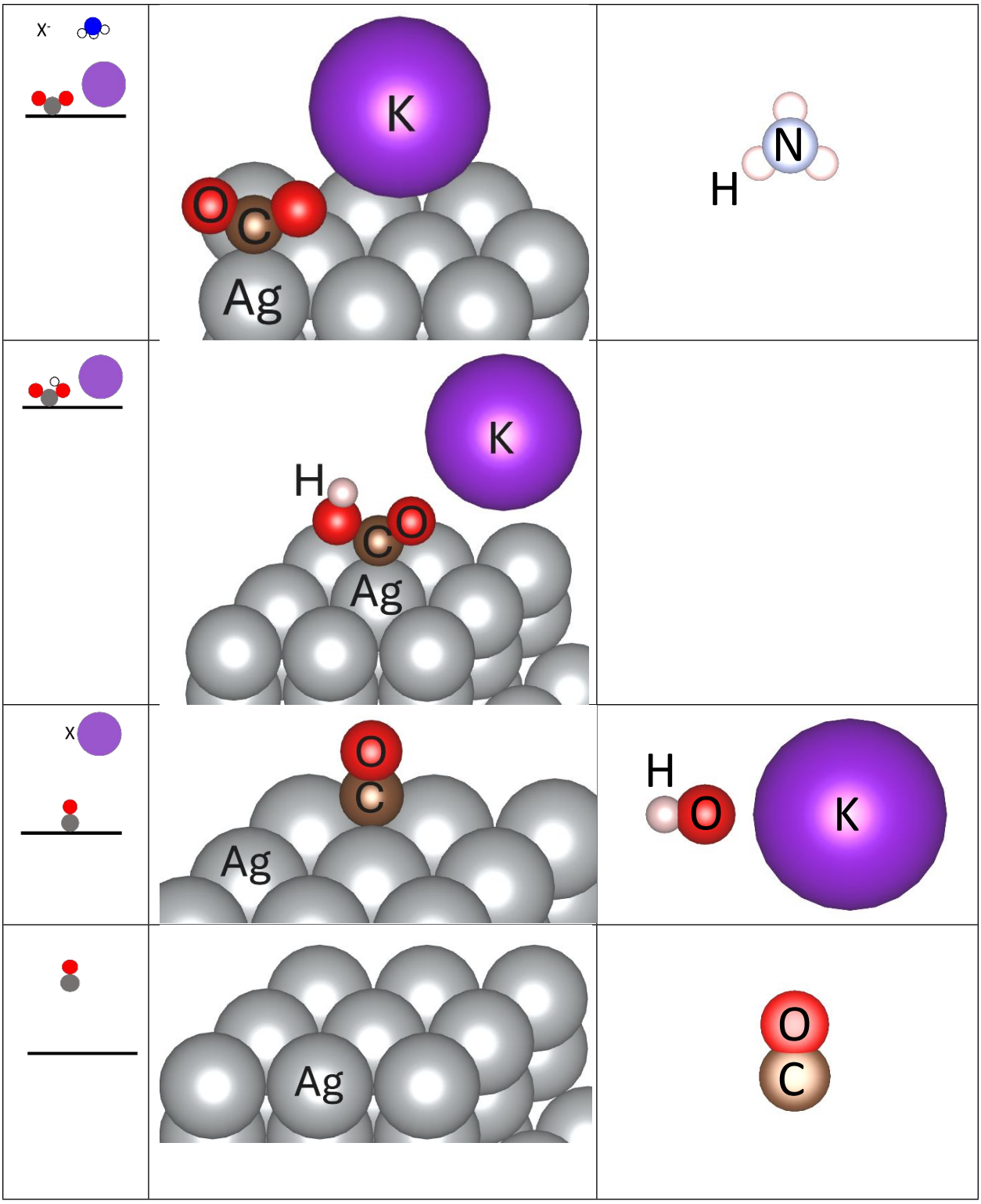
X-
K
O
C
Ag
N
H
K
H
O
C
Ag
X
O
C
Ag
H
O
K
Ag
O
C

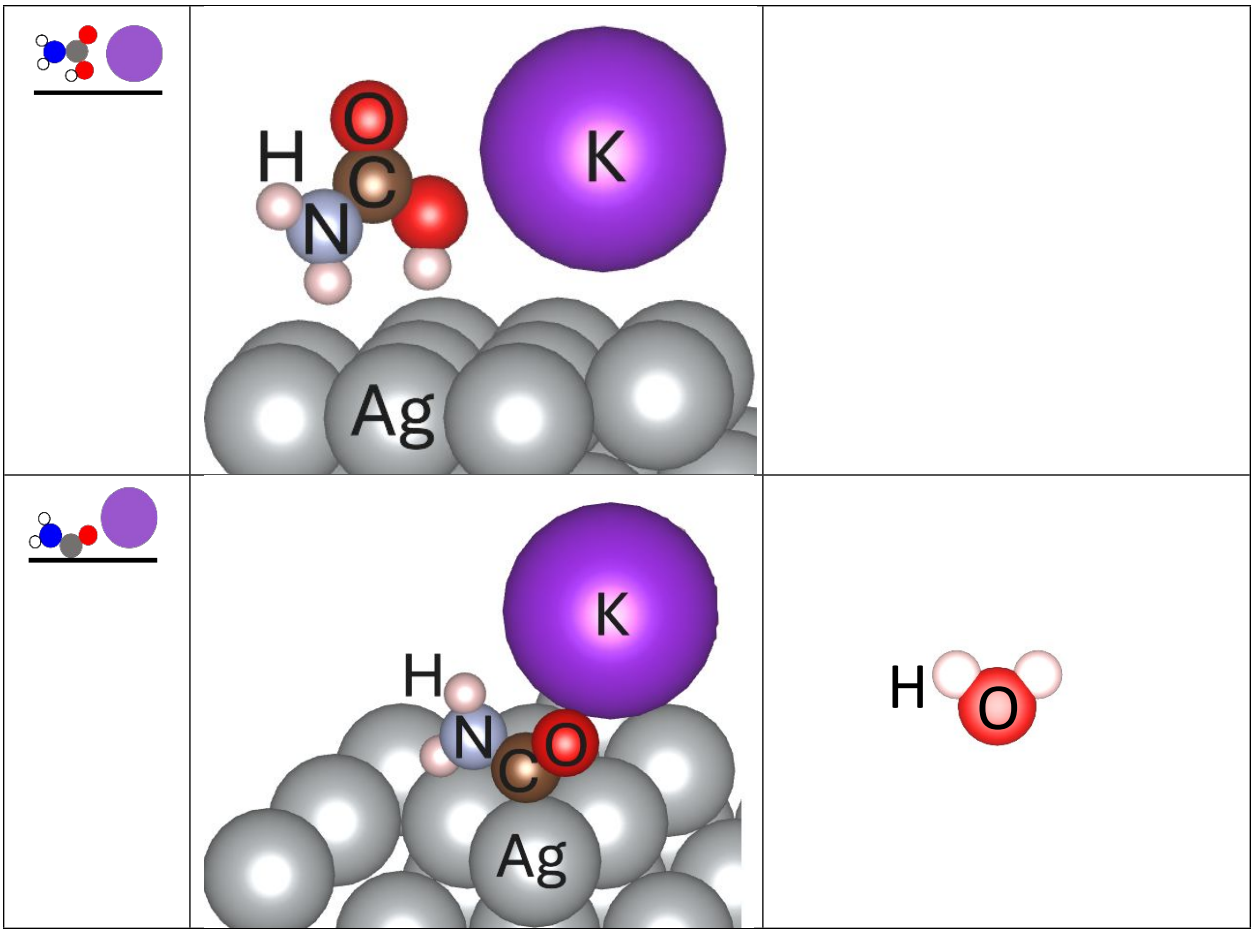

As stated, the captured CO_2 is an anion. Thus, to bring the negatively charged anion to the cathode it is accompanied by a cation. It has also been shown that for MEA captured CO_2 the presence of the cation assists in the electron transfer to the captured CO_2 anion.[29] At this point two processes can occur: the capture agent can be initially removed by C-N bond cleavage, and CO_2 is reduced (initial R-C cleavage, top branch in Figure 5) or the complex can be directly protonated while the C-N bond is cleaved at the end to generate CO (final R-C cleavage, bottom branch in Figure 5).

For the initial R-C cleavage, the captured CO_2 is first adsorbed to the catalyst and electrochemical decomposed to reform the capture agent and adsorbed CO_2. A second PCET occurs to form COOH*. At this point both free electrons have been used, so the final protonation to convert COOH* into CO must be done thermally. To complete the cycle CO desorbs. For the final R-C cleavage, the complex is first electrochemically protonated. A second PCET occurs to cleave the C-O bond forming H_2O. However, similar to the initial R-C cleavage, at this point both electrons have been used, and the final protonation is done thermally to complete the cycle.[31]

It is necessary to consider two protonation steps as electrochemical and one protonation step as chemical. However, it is not trivial to determine what step in the mechanism corresponds to the chemical protonation. Equation 4 and Figures 4 and 5 summarize why the c-CO_2RR is highly

proton source dependent. As compared to the HER and CO_2RR, one more protonation is necessary which cannot be assisted electrochemically.

Previous work explored the carbonate reduction to formic acid on oxide-derived Cu. They also found that two of the protonation processes were done electrochemically, while the third was done thermally. However, they found that the first PCET was to place a surface hydride onto the surface. They then conducted a thermal protonation of the adsorbed carbonate to form adsorbed bicarbonate. This bicarbonate and the surface hydride then reacted to form bound formate and H_2O. A final PCET occurred to form formic acid.[32] Their proposed mechanism offered a different approach to the c-CO_2RR as to our knowledge no work has proposed a surface hydride in the c-CO_2RR mechanism.

Another recent work explored the production of methane from the direct reduction of carbamic acid into methane on Ni supported on Au.[116] From the low coverage of Ni (~5%), the authors assumed that Ni is in the form of single atom alloy of Ni in Au. Sykes *et al.* previously showed the formation of single atom Ni alloys in Au.[117] Their reaction pathway using a Ni atom substituted at the Au(211) surface is shown as Figure 6.

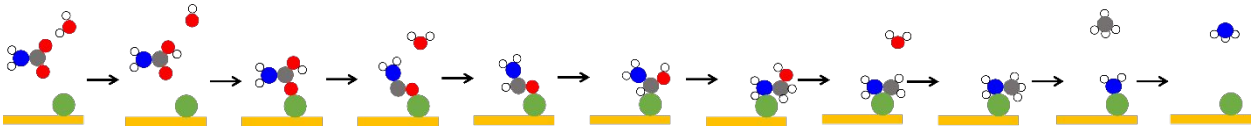

Figure 6: Cartoon of the proposed mechanism of carbamic acid reduction to methane on Ni single atoms supported on Au. A similar mechanism was determined on pure Ni. The yellow slab represents the Au(211) surface, the green atom is Ni, red atom is O, blue is N, grey is C, and white is H. Adapted from:[116]

Table 2: Structures used in previous work that corresponds to the cartoon pathway in Figure 6

Cartoon	Part on Surface	Part in Solution
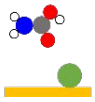	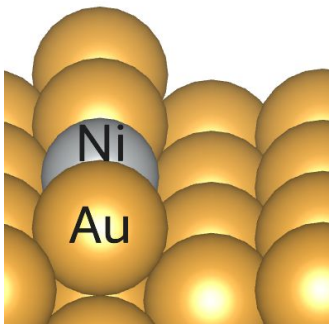	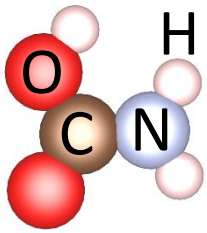

	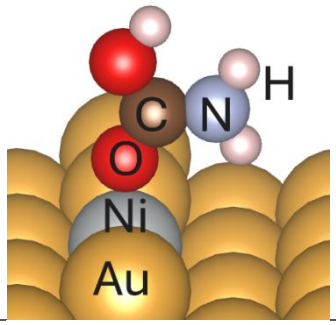 H C N O Ni Au	
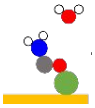	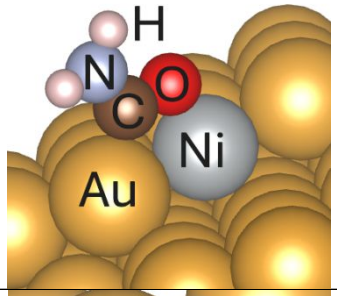 H N O C Ni Au	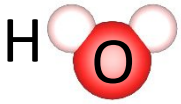 H O
	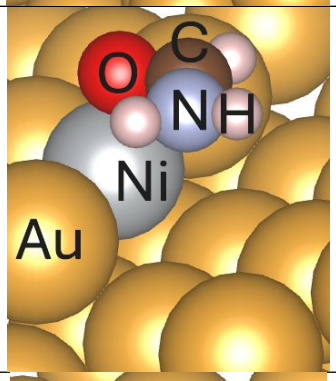 C O N H Ni Au	
	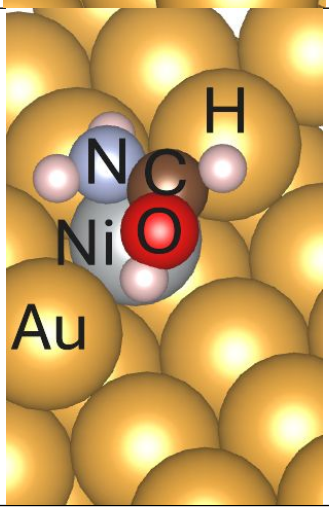 H N C Ni O Au	

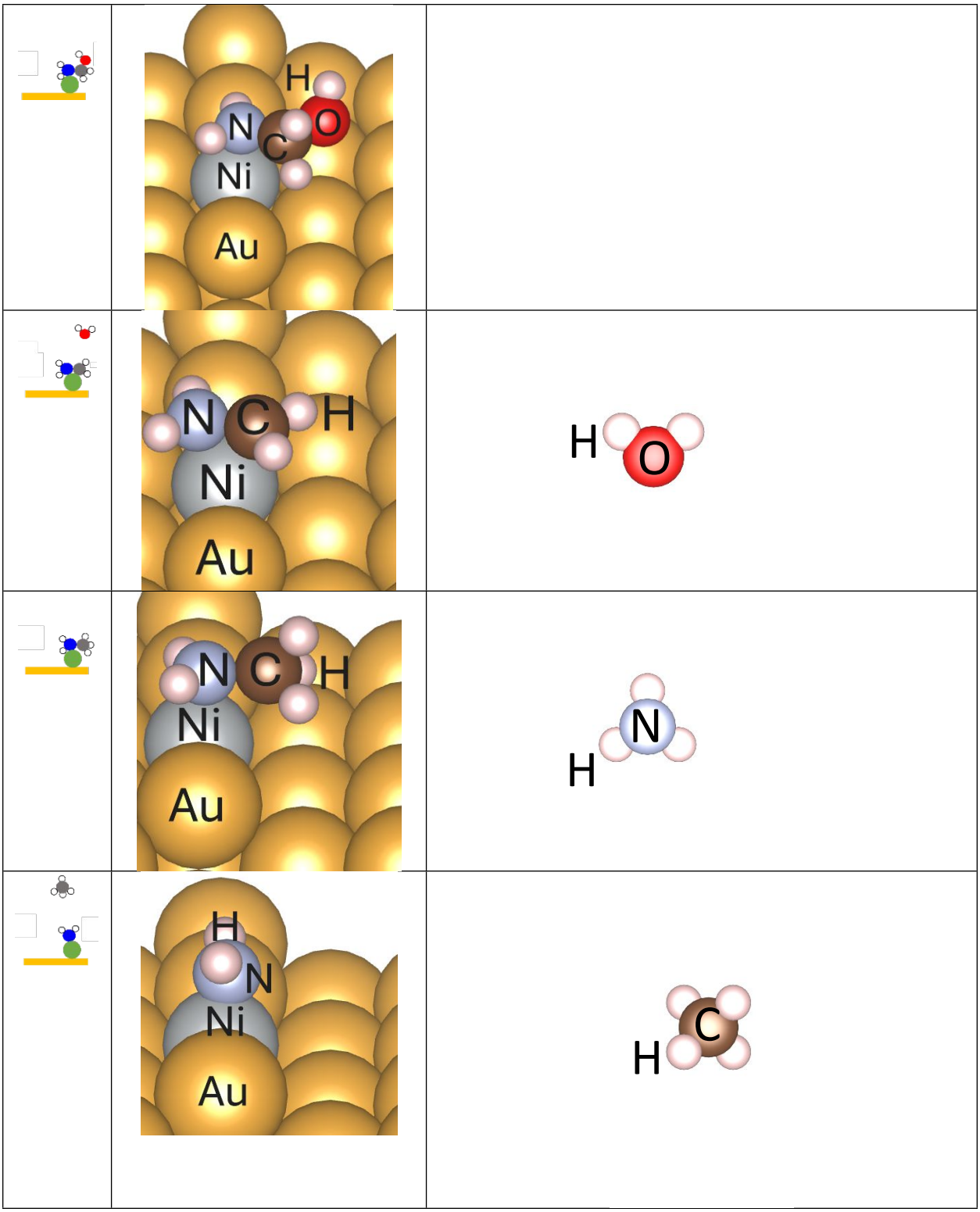
H
N
C
O
Ni
Au
N
C
H
Ni
Au
H
O
N
C
H
Ni
Au
H
N
H
H
N
Ni
Au
H
C

They argue that the carbamate undergoes an outer shell proton transfer to form carbamic acid which adsorbs to the surface, and thus they do not model an explicit cation as well. After this proton transfer the carbamic acid adsorbs to the surface and undergoes 8 PCETs, similar to the CO_2 reduction to methane as discussed in Section 2.1.2.1. As shown in Figure 6, the capture agent (in this case -NH_2) does not participate in the reaction until the final protonation to reform the capture agent in the final step. Similar to the CO pathway an additional protonation is needed to convert the carbamate into methane as compared to the CO_2RR. However, they consider the thermal protonation to be the outer shell proton transfer, the first protonation. Thus, for the three mechanistic studies on CO, formic acid, and methane production, different protonations were done thermally, meaning further studies are needed to explore this thermal protonation and the governing factors that affect its location.

2.2.3 Comparison and Further Work Needed

As the c-CO_2RR is a far more complex reaction than the CO_2RR further work needs to be conducted on completely elucidating its reaction pathway depending on the desired product. For pathways leading to CO, aspects to understand the nature of the surface in reaction conditions, including for example the effect of co-adsorbed hydrogen atoms is lacking. For pathways leading to formic acid, further elucidation of the overall pathways would be required. For pathways leading to methane, further evaluation of potential dependence on the reaction pathway is needed. With all pathways reported a true kinetic analysis is lacking. Importantly, however, both the CO and formic acid reaction studies show that only two electrons can be transferred per cycle, necessitating a chemical protonation, and thus providing further evidence for the validity of equation 3. In the case of methane, nine protonations and eight electrons were available as compared to the eight PCETs were the methane directly produced from CO_2. Additionally, while current research primarily addresses the thermodynamics of identifying which steps are chemical versus electrochemical, further kinetic modeling would be invaluable for a comprehensive understanding of the pathway. However, this modeling requires a reasonable interfacial model to accurately describe the reaction environment, a topic which will be discussed further in Section 4.

2.3 Hydrogen Evolution Reaction (HER)

The HER is a common undesirable side reaction that occurs in reductive conditions. The HER has two different mechanisms: Volmer-Heyrovsky and Volmer-Tafel. Equations 5-7 show these various steps while equation 8 shows the overall reaction.[118]

$$(H^+ + e^-) + * \rightarrow H* \quad \text{(Volmer Step)} \quad (5)$$

$$(H^+ + e^-) + H* \rightarrow H_2 + * \quad \text{(Heyrovsky Step)} \quad (6)$$

$$H* + H* \rightarrow H_2 + 2* \quad \text{(Tafel Step)} \quad (7)$$

$$2(H^+ + e^-) + * \rightarrow H_2 \quad (8)$$

The Volmer-Heyrovsky mechanism is a 2-step process where first equation 5 occurs and then equation 6, while the Volmer-Tafel mechanism is a 3-step process where equation 5 occurs twice. Then equation 7 occurs to finish the process and desorb H_2.

2.4 Accounting for Various Proton Sources

The hydrogen electrode method can be used to model the chemical potential of the coupled proton and electron ($\mu_{(H^+ + e^-)}$) and is shown as Equation 9.[119,120] In this method the chemical potential of a coupled proton and electron (referenced to SHE) is taken as a function of potential, temperature, solution pH, and the free energy of H_2 at 1 bar (Equation 9).[21]

$$\mu_{(H^+ + e^-)} = \frac{1}{2} * \mu_{(H_2)} - e * U - ln(10) * k_B * T * pH \quad (9)$$

However, in the c-CO_2RR, CO_2RR, and HER various proton sources are present. It is not fair to assume that each proton source provides a coupled proton and electron with identical chemical potentials. Additionally, it is known that the pH near the electrode is different from the bulk,[121,122] and thus, choosing the pH to plug into equation 9 becomes an issue.

To account for this, it has been determined that for a coupled proton and electron the chemical potential can be defined by the proton source's pK_a.[31] This accounts for different proton sources with smaller pK_a values being more active toward donating their protons.

To explain this, point a worked example follows. Consider the protonation of CO_2 by H_2O. Equation 10 shows the overall reaction.

$$H_2O + e^- + CO_2 * \rightarrow COOH * + OH^- \quad (10)$$

An equilibrium will exist based on the proton source's pK_a In this case pH = pK_a = 14.[123]

$$H_2O \leftrightarrow H^+ + OH^- \quad (11)$$

Thus, combining equations 10 and 11 yield equation 12.

$$H^+ + e^- + CO_2 * + OH^- \rightarrow COOH * + OH^- \quad (12)$$

Thus, $H^+ + e^- = H_2O - OH^- + e^-$ at with respect to the pK_a of H_2O. Therefore, equation 9 becomes equation 13. Conveniently, this method can be extended to all proton sources.

$$\mu_{(H^+ + e^-)} = \frac{1}{2} * \mu_{(H_2)} - e * U - ln(10) * k_B * T * pK_a \quad (13)$$

Figure 7 plots the computationally determined equilibrium potentials of the HER, CO_2RR to CO and c-CO_2RR to CO as a function proton source pK_a the equilibrium potential is defined as the potential at which the overall reaction free energy goes to 0. The equilibrium potentials are defined by solving equations 14-16 for a given proton source pK_a. R and X are defined in section 2.2. Equation 13 is substituted for $\mu_{(H^+ + e^-)}$ in equations 14-16 for a given proton source.

$$\mu_{H_2} - 2\mu_{(H^+ + e^-)} = 0 \quad (14)$$

$$\mu_{CO} + \mu_{H_2O} - \mu_{CO_2} - 2\mu_{(H^+ + e^-)} = 0 \quad (15)$$

$$\mu_{CO} + \mu_{H_2O} + \mu_{KX} + \mu_{RH} - \mu_{KRCO_2} - 2\mu_{(H^+ + e^-)} - \mu_{XH} = 0 \quad (16)$$

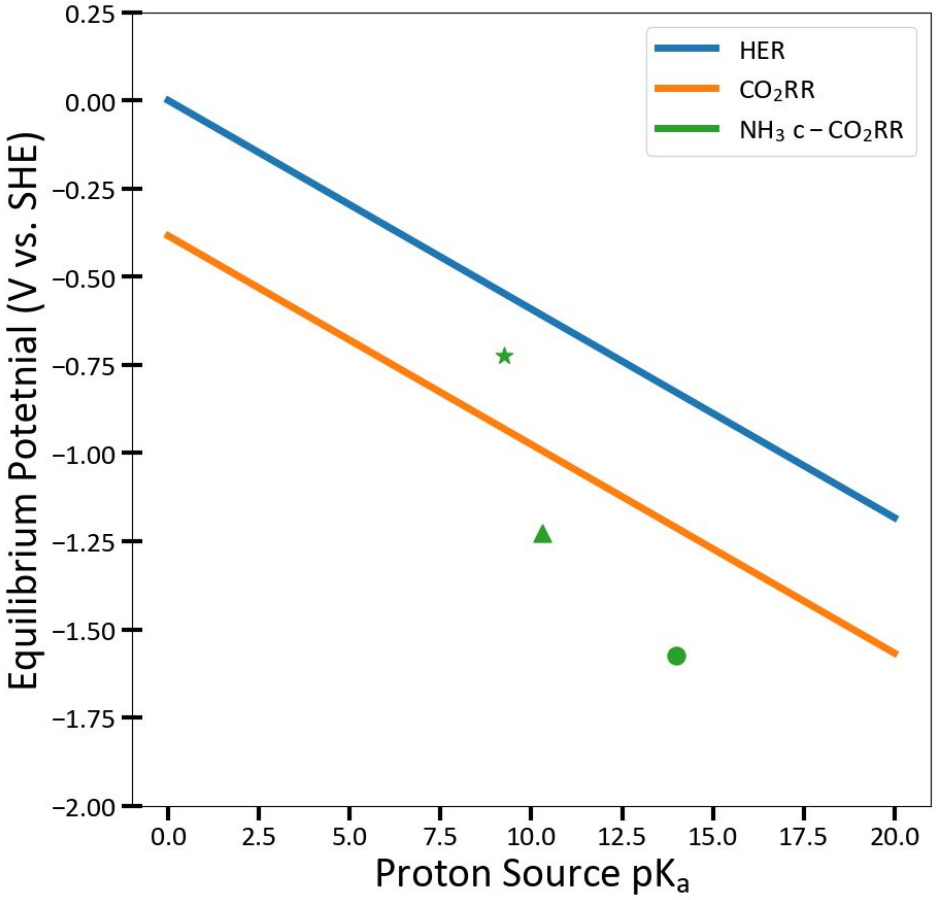

Figure 7: Computationally reported equilibrium potentials for the HER (blue), CO_2RR (orange), and NH_3 c-CO_2RR (green) as a function of proton source pK_a. The various shapes for the c-CO_2RR represent the different proton sources reported (star = NH_4ClO_4, triangle = $KHCO_3$, and circle = H_2O). Adapted from: [31]

Figure 7 shows that thermodynamically, the HER is the most favorable reaction and typically the c-CO_2RR is the most difficult reaction thermodynamically. It is noted that when NH_4ClO_4 is used as a proton source the c-CO_2RR becomes thermodynamically more favorable than the CO_2RR. From equations 1, 2, and 8 the CO_2RR and HER dependence on the proton source appears only in determining the chemical potential of the proton and electron. However, having both electrochemical and chemical steps present in the c-CO_2RR leads to the proton source

dependence appearing in both the chemical potential of the proton and electron as well as in the products via the resultant salt. Therefore, it is likely that the nature of the resultant salt generated by the NH_4ClO_4 proton source differs from the resultant salts generated from the $KHCO_3$ and H_2O sources. This leads to a non-linear relationship between the proton source pK_a and equilibrium potential. Therefore, further work is needed to fully understand the role the proton source has on the thermodynamics and kinetics of the c-CO_2RR. However, even with the benefits that the NH_4ClO_4 proton source provides, the HER is still thermodynamically more favorable than the c-CO_2RR. Therefore, it is imperative to choose a catalyst the severely hinders the HER kinetically, while provides reasonable kinetics for the c-CO_2RR and the CO_2RR.

3. Accounting for the potential and pH in the modelling of c-CO_2RR and other electrochemical reactions

In all electrochemical reactions it is important to correctly model the potential. Currently there are two main methods of accounting for the potential.

3.1 Computational Hydrogen Electrode (CHE) Model

The CHE Model developed by Nørskov *et al*. considers potential dependence in only the coupled proton electron transfers, and no potential dependence in non-electrochemical steps such as adsorption and desorption.[119] Thus, the internal energy of the various intermediates are not considered as a function of potential.

Thus, this method provides a simple way to calculate the reaction pathway of an electrochemical process. However, it does not take into account the potential dependence of the surface adsorbed intermediates. Another drawback of using the hydrogen electrode model is that it forces the proton and electron to be coupled. Thus, it cannot accurately be used to explain the energy difference of a decoupled proton-electron transfer, such as if a charge transfer occurs during CO_2 as proposed by Shen *et al*.[41] Some literatures have proposed that the CO_2 adsorption is indeed an electrochemical step, which the CHE model cannot properly model.[46,124] Thus, it has been proposed to use grand-canonical methods.[47]

3.2 Surface Charging

For a better description of potential influence in the modelling, it is necessary to consider how the Gibbs free energies of intermediates and transition states are influenced by the potential. In this method, the proton and electron transfer do not need to be coupled, allowing for a more accurate description for complex charge transfers, such as CO_2 adsorption.

Additionally, during the c-CO_2RR, the role of the cation is important and dynamic. Originally, the cation interacts with the negatively charged captured CO_2. However, depending on the charge of the intermediate the role of the cation changes. For example, if the more common

final R-C cleavage pathway (Figure 5) if taken then the original negatively charged captured CO_2 (RCO_2^-) will be protonated to form a neutral RCOOH. This leads to a weaker interaction between the complex and the cation and a stronger interaction between the cation and the surface. Chemically it was observed that there was a large shift in the PZC between these intermediates. It was further hypothesized that this shift in PZC, coupled with the PCET leads to an electrochemical step with little potential dependence. Additionally, the cation is involved with the overall reaction and is active in the chemical step (Figure 5). Thus, a similar coupled process occurs on the chemical step. Therefore, it is imperative that Gibbs free energy is a function of potential.[31]

In the surface charging method, the entire system is modeled as a capacitor, the electron is decoupled from the proton, and the reference potential is vacuum.[125] Therefore, the energy of an electron in vacuum is set to 0. The work function is defined in equation 17.[126]

$$\Phi = eU_{vac} - E_{fermi} \quad (17)$$

Φ is the work function, U_{vac} is reference potential in vacuum, e is the charge of an electron, and E_{fermi} is the energy at the Fermi level.

However, experimentally, the standard reference potential is the standard hydrogen electrode (SHE). To convert between the vacuum potential and the SHE potential, one needs to subtract 4.44 ± 0.02 V from the vacuum potential to obtain the SHE potential as shown in equation 18.[127,128]

$$U_{SHE} = \frac{\Phi + E_{fermi}}{e} - 4.44 \quad (18)$$

To find the free energy as a function of electrode potential, the free energy is first expanded as a Taylor Series about the free energy at the potential of zero charge (PZC). It is typically assumed that a second order approximation is accurate enough. The work function can also be defined as the derivate of the free energy as a function of charge. Assuming that a constant capacitance then the second derivative of the electronic energy can be taken as the inverse of the capacitance. Thus, the free energy can be written in terms of capacitance (Equation 19)[125] where E is the free energy at the electrode potential at interest, E_0 is the free energy at PZC, C is the capacitance, Φ is the work function at the potential of interest, and Φ_0 is the work function at PZC.[125]

$$E = E_0 + C(\Phi - \Phi_0)\Phi_0 + \frac{C(\Phi - \Phi_0)^2}{2} \quad (19)$$

By applying equation 18 the free energy can be written as a function of potential (Equation 20).

$$E = E_0 + C * \Delta U_{SHE} * e * \Phi_0 + \frac{C*(\Delta U_{SHE}*e)^2}{2} \quad (20)$$

Where ΔU_{SHE} is $U_{SHE} - U_{SHE0}$ where U_{SHE} and U_{SHE0} are the electrode potentials at the desired potential and PZC, respectively. Φ_0 is defined by the equation 21.

$$\Phi_0 = (U_{SHE0} + 4.44) * e - E_{fermi} \quad (21)$$

This is important as it allows for a description of the free energy as a function of potential. It is important to note that an assumption in this equation is that the capacitance of the modeled capacitor is constant. This is typically valid but breaks down as the charge becomes far from the PZC.[125]

Using this method is simple. A set of optimizations is done at different injected charges to change the work function. This allows a parabola to be fit to the equations above. This does mean that the geometry is now important, as identical adsorbates with different binding modes will lead to different difference capacitances. Thus, multiple parabolas can be drawn for the same intermediate. Therefore, when using this method, it is imperative that a thorough configuration search is conducted to ensure that the global minimum energy is found.

As an example, the SC method has also been used to explore the oxidation of formic acid into CO_2 (effectively the reverse CO_2RR to formic acid).[129] They found that the CHE and SC provide the same trend in free energy along the reaction pathway. They found that the free energy values of each of the intermediates and transitions states were within 0.1 eV for most of the states. However, for some of the states, the SC and CHE method differed more than 0.1 eV, with the largest difference being the transition state to rotate the adsorbed formate. The SC method was determined to produce a value about 0.3 eV more stable than the CHE method.[129]

The authors also noted that the reorientation of the adsorbed formate, as well as the desorption of CO_2 were potentially dependent.[129] Although the reorientation of formate was not considered in any of the c-CO_2RR literatures at this point, the adsorption of CO_2 was found to be potentially dependent in previous work.[31,130,131] Thus, this agreement further highlights the need for more advanced treatment of the potential beyond the CHE model for the c-CO_2RR.

It is further interesting to consider the differences in charge injection. For the CHE model the charge injection occurs in unit intervals and only changes when a PCET occurs. However, in the SC method, the injected charge can change for each intermediate. They find that the charge injection can differ between the SC and CHE methods by over 0.5 charge, and that the states with the largest differences in injected charge were typically states associated with formate rotation or CO_2 adsorption. Thus, these processes have some charge dependence which the SC method captures, but the CHE method misses.

3.3 Cell Extrapolation

The surface charging method uses a grand canonical ensemble which means that there is an external reservoir of electrons that the systems can exchange with which leads to a constant potential. However, another method for calculating the potential is called cell extrapolation. In this method a series of calculations using different sized unit cells of the same intermediate is performed.[132] In experimental conditions, the reaction is conducted at constant potential. However, until recently, simulations occurred at constant charge (some codes such as VASPSol++ and JDFTx are able to conduct simulations at constant potential).[133,134] Chan and Norskov showed that the change in charge from an initial state (IS) to a final state (FS) for a surface reaction can lead to

potential differences of over 2V. However, they showed that as the super cell of the simulation increased, this potential difference between the IS and FS decreased, and in the limit of infinite cell size the difference in potential would be 0.[135] Given that the computational cost of a DFT calculations scales close to the cube of the system size, the major drawback of this method is that it can be computationally slow given that multiple calculations with different unit cell sizes need to be conducted for the same intermediate.[132]

3.4 Charge Extrapolation

Unlike the cell extrapolation method, which requires multiple calculations of various unit cell sizes, the charge extrapolation method involves calculating the change in charge between states since the change in charge is proportional to the change in potential. However, deciding which charge to use is challenging.[132] Previous work considered the sum of the Bader charge of the slab and the adsorbates. They define adsorbates as any atom interacting with the surface. For example, on the Heyrovsky step, in the IS, the Bader charge includes the H adsorbed which will undergo the Heyrovsky step to form H_2. However, on the TS and the FS, the charge on this H is not included as it has become H_2. Chan *et al*. showed that the charge extrapolation and cell extrapolation method provide similar results.[135]

4. Modeling techniques typically used in modeling the c-CO_2RR and other electrochemical reactions

4.1 Implicit Solvent

4.1.1 Polarizable Continuum Model (PCM)

A simple method to model the effects of solvation is to implicitly model the solvent as a Polarizable Continuum Model (PCM) defined by its dielectric constant. In this model, the solvent molecules are modeled in a continuum rather than explicitly. In this method, the solvation free energy is treated as the sum of the electrostatic free energy, dispersion-repulsion free energy, and the cavitation free energy.[136] By treating the solvent as a continuum rather than individual molecules the computational cost is significantly reduced.

When an electrochemical reaction occurs in solution, there must be an electrolyte present. To model the electrolyte the linearized Poisson-Boltzmann equation (LPBE) is commonly used. This equation relates the electrostatic potential to ions in the electrolyte's charge density the via the Debye Screening length, a parameter dependent on the solution dielectric constant, temperature, and concentration of electrolyte.[137]

There are many approximations in this method, the most glaring being that it ignores any local chemical interactions between the solvent and the adsorbates. For example, cations typically form solvation shells in aqueous environments, and the structure of these shells can vary significantly depending on the cation.[138,139] This solvation chemistry can also affect the interactions with adsorbates. It has been proposed that larger cations such as K^+ and Cs^+ can

interacted with CO_2 in a different configuration than Li^+ and Na^+, thus leading to increased CO_2RR activity with the larger cations.[35] However, a pure implicit solvent cannot explicitly capture the solvent's interaction with the explicitly modeled cations nor the solvent's interactions with the adsorbates, and therefore, it is important to benchmark if implicit solvation is appropriate for the particular system. As shown in Figure 8, Steinmann *et al*. used various solvation models to explore the change of pyridine binding mode on Au(111).[140]

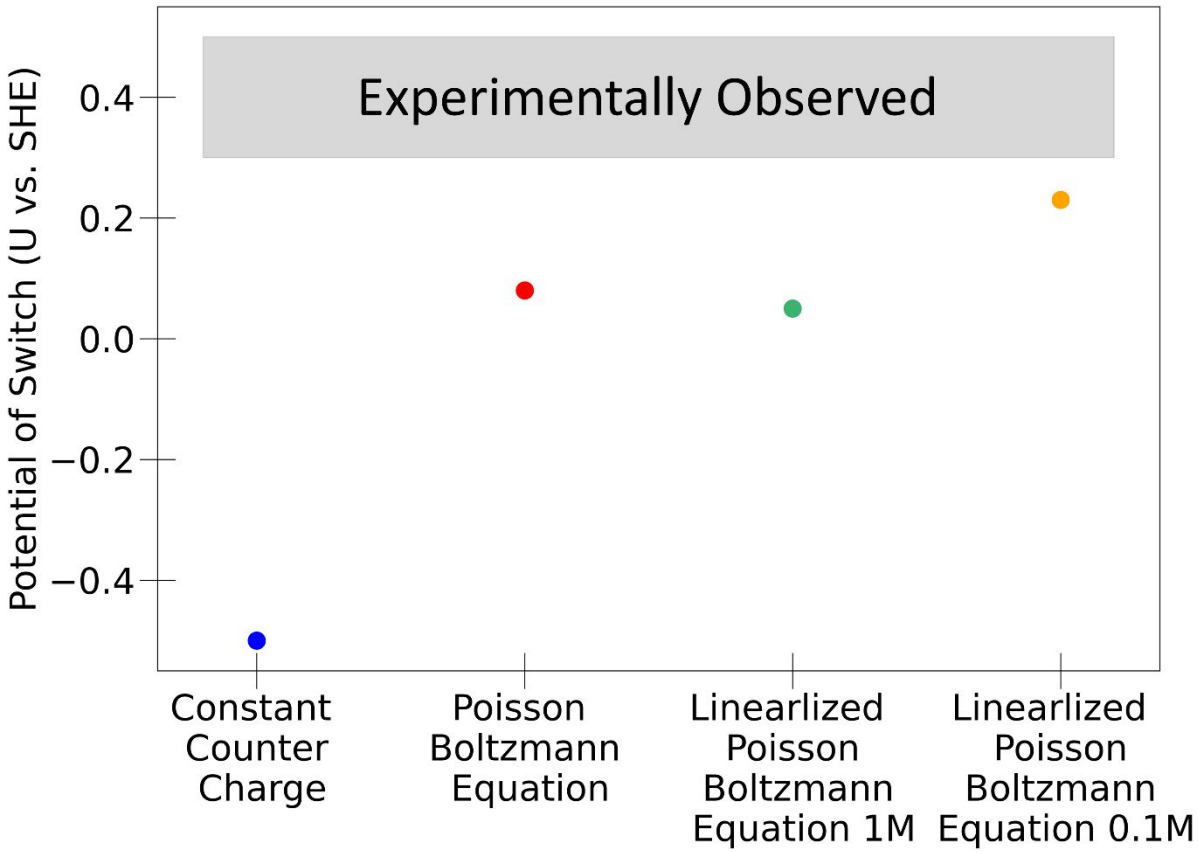

Figure 8: Computationally and experimentally observed potential at which the binding mode of pyridine switches on Au. At more positive potentials, the pyridine is known to bind perpendicular to the Au surface, while at more negative potentials, the pyridine binds parallel to the Au surface. The grey region represents the potential region in which the shift is experimentally known to occur. The points represent four different modeling cases, that build upon the complexity. Orange is the same set up used in VASPSol, assuming the user inputs a realistic concentration of ions.

Previous work by Steinmann *et al*. explored the electrochemical change in pyridine binding mode on Au using the surface charging method and various counter charge distribution models and compared the results to experiment.[140] Figure 8 shows the performance of the various models they used. Experimentally, it is known that pyridine will adsorb perpendicular to the Au surface at more positive potential. When the potential is about 0.3 V to 0.5 V vs. SHE a shift in binding mode is known to occur where the pyridine will adsorb parallel to the Au surface (grey bar). Initially,

the authors used the surface charging method and applied a uniform counter charge. They were able to observe this qualitative binding mode shift, but they found the shift occurred at about -0.5 V vs. SHE (blue point), at least 0.8V more negative than the experimental value. They then applied an electrolyte distribution modelled via the Poisson Boltzmann equation. Qualitatively the shift correctly occurs again, but at a far more positive potential of 0.1 V vs. SHE (red point), in much better agreement with experiment.

However, to properly account for the concentration of electrolyte, they use the LPBE. They show that with a default value of 1M of electrolyte, the shift occurs at about 0.05 V vs. SHE (green point). However, by applying the correct concentration of the electrolyte of 0.1M, they were able to observe the shift at about 0.2 V vs. SHE (orange point), close to the experimental range of 0.3 to 0.5 V vs. SHE.[140] In VASPSol the electrolyte distribution is treated by the LPBE.[137] Therefore, assuming that the user uses a realistic concentration of electrolyte, this test case shows a good agreement between the theoretical calculations and the experimental observations.

As most c-CO_2RR work has been done using the Vienna *ab-initio* Simulation Package (VASP)[141,142] in this review, we will focus the methods used in VASPSol and VASPSol++,[133,136,137] an add-on to VASP that allow for implicit solvation calculations.

4.1.2 VASPSol and VASPSol++

As stated, one of the most common implicit solvation packages are add-ons for VASP named VASPSol,[136,137] and a newer version named VASPSol++.[133] In this package the solvent is modeled as a continuum dielectric medium defined by the dielectric constant of the solvent. The program assumes that the dielectric constant is truly a constant.[136] Realistically, the dielectric constant is a function of position.[143]

In VASPSol all explicit atoms are treated at solute in the continuum. Thus, a cavity must be created to place the solute in the medium. Typically, three main parameters define the cavity: the surface tension, the electron density at the edge of the cavity, and the cavity's width.

Typically, the electron density at the edge of the cavity and the width of the cavity can be taken as the default values of 0.0025 $Å^{-1}$ and 0.6, respectively.[136] Careful examination needs to be taken to ensure that the implicit solvent is not populating an area it should not. The final parameter is the surface tension of the cavity. It is difficult to define this value as it is not a physical value, but an implicit one in the solvation model. Therefore, there is typically no experimental bench marking to assist in choosing a surface tension. Fortunately, previous work has shown that changing the surface tension has small effects on electrochemical results. Therefore, a value of zero is typically taken.[144]

In the case of an electrochemical system, there will be some electrolyte that needs to be modeled. In VASPSol, this is taken as a density of counter change applied in the solvent continuum.[145] The linearized Poisson-Boltzmann equation (LPBE) models the counter charge via the electrolyte's Debye screening length. The Debye screening length is a function of temperature, electrolyte concentration, and solvent dielectric constant.

In the VASPSol package there are three additional main assumptions. Firstly, it is assumed that the Poisson-Boltzmann equation can be perfectly linearized. This is mainly true, but at highly negative potential this assumption could break down. The other assumption is that the distribution of electrolyte is uniform. Similarly, to the dielectric constant this is a function of space and time. The final assumption is that neither the solvent nor the electrolyte occupies any volume.[143] What is done is to decay the solution of the PCM and the LPBE to zero in the regions outside the solute and to have them go to one in the regions assumed to be bulk electrolyte.[133] Therefore, careful consideration needs to be made in choosing the electron density at the edge of the cavity. In certain systems it is possible for the implicit solvent and electrolyte to "leak" into cavities that are not physically accessible in a realistic solution.[133]

It is to be noted that there is an update version of VASPSol named VASPSol++ that offers some improvements.[133] In VASPSol++, several parameters can be defined to more accurately defining the solvent and electrolyte. In this method the solute is defined by a van der Waals volume where no solvent is allowed to enter. The solvent is also defined by a van der Waals volume which is defined by the radii of the solvent. In this case solvent will occupy all regions of space in which the van der Waals volumes of the solute and solvent do not overlap. To properly account for the charge distribution of the solvent, an additional parameter the dielectric radius is defined to account for the dielectric response the solvent has on the solute past the boundaries the solvent can occupy. To model the electrolyte, the radius of the electrolyte is taken to define the region of space where the electrolyte can occupy.[133] The final difference is the value for the surface tension for the formation of the cavity. As stated in VASPSol, there is very little benchmarking for the surface tension. In VASPSol++, the surface tension is taken to be a function of solvent molecule and dielectric radii. However, for all these parameters, careful benchmarking needs to be conducted to accurately model the solvent and electrolyte. To determine the van der Waals radii of the various components it is recommended to take the isosurface where the cavity function has a value of 0.5. The most difficult parameters to parameterize is the dielectric radius. They find that in some certain cases the dielectric radii necessary to match computational results to experiments is unphysical. Therefore, they recommend a value of 1 Å as there is little benchmarking at this point, similar to how the surface tension is set in VASPSol.[133] However, unlike VASPSol where it has been shown the value chosen for the surface tension has little effect on the results,[144] there is no benchmarking yet on the effects on the dielectric radius on the results. As VASPSol++ is a new program, not a lot of literature exists using it. Therefore, further work needs to be done to systematically define all the necessary parameters needed to accurately describe the solvent and electrolyte.

However, even though there is not a lot of literature using VASPSol++ yet it does provide significant benefits over VASPSol. In addition to more accurately accounting for the solvent and electrolyte's volumes, another feature is the ability to run constant potential calculations.[133] Within the current VASPSol framework several grand canonical DFT (GC-DFT) calculations are conducted to fit equation 20 so that the free energy can be represented as a function of potential. However, if the desired potential is known then time can be saved. This has the potential to improve calculations such as activation barrier calculations.[133] Therefore, in our estimation, both VAPSSol and VASPSol++ serve distinct purposes. However, currently, literature involving

solvation models in VASP used VASPSol, and thus this work mainly covers VASPSol. However, further work is needed on using and benchmarking VASPSol++.

4.1.3 JDFTx

Another code that does grand-canonical DFT (GCDFT) is JDFTx.[134] In VASPSol and VASPSol++,[130,134] the implicit solvent is treated as a polarizable continuum model (PCM).[133,137] However, in JDFTx there are various solvation method available such as the charge-asymmetric nonlocally determined local-electric (CANDLE) method,[146] the spherically average liquid susceptibility *ansatz* (SaLSA), as well as classical DFT.[147]

Bossche *et al*. explored the activation barriers for the HER using both VASPSol and JDFTx. They found that the difference in barriers is typically less than 5%. However, the largest percent difference in barriers is around 25%.[148] To our knowledge no works have explored using JDFTx for the c-CO_2RR.

4.2 Explicit Solvent

Although implicit solvation is nice since it is relatively computationally inexpensive, the lack of explicit consideration of the solvent can have limitations. As stated, it is known that cations will form hydration spheres.[138,139] Solvation models with implicit solvation is approximate. Using the surface charging method with an implicit model of the solvent and of the electrolyte provides a simple model of the electric double layer (EDL). In the VASPSol code, the solvent is modeled as a polarizable continuum model (PCM) based on the dielectric constant and the electrolyte is modeled as solutions to the LPBE using the Debye Screening Length as the main variable.[136,137] VASPSol++ improves the cavity definitions for the solutes, but the solvent is still modeled as a PCM and electrolyte is still modeled as a solution to the LPBE.[133] This type of model has been shown to be effective when the focus of the modeling is on the adsorbate. However, if the goal is to explore the chemistry of the EDL, then it is necessary to use explicit solvation.

Experimentally, a region termed the EDL is known to form around the electrode surface. This occurs because the charged electrode will attract ions of the opposite charge. These ions in turn will attract ions of the opposite charge.[149] As the c-CO_2RR is still in its infancy, most research has focused on exploring the feasibility of different catalysts and capture agents through the use of implicit solvent and electrolyte. This combined with the large computational cost associated with explicitly modeling the EDL has led to no known works to be published on explicitly modeling the EDL during the c-CO_2RR. However, in the c-CO_2RR, it is known that some of the cations present can also act as proton sources.[31,150] Therefore, further study into the nature of the EDL is necessary. For the purposes of this tutorial, we will briefly explore how the EDL has been previously explicitly modelled.

Since proper modeling of the EDL requires explicit modeling of the solvent-electrode interface, molecular dynamics (MD) approaches have appeared as a potential method to sample

the configurations. Given the large size of the simulation supercell, force fields are typically employed in this modeling. Previous works have used Lennard-Jones parameters, AMBER forcefield[151,152] and GAL17[153,154] (with a newer version GAL 21 being available currently).[155] These methods have been used to model the energy penalty to move solvent molecule aside so that an adsorbate can be placed onto the surface.[153]

Recently, Guan *et al.* used *ab-initio* MD to explore the nature of EDL in the presence of acetone and methylamine. They were able to show that the capacitance and polarizability was dependent on the molecule present in the double layer.[156]

In the context of the c-CO_2RR this is important as a cation is present. Previous works have used the implicit solvation model,[31,33] but it would be interesting to compare the effects of an explicit solvent model on the reactivity determined by implicit solvent. The other issue is that the adsorbates in the c-CO_2RR react with molecules in solution, which are proton sources. Therefore, any barriers calculations must include some degree of explicit solvent.

Several computational techniques are employed to incorporate explicit solvents in catalysis modeling, like static water layer modeling, molecular dynamics simulations, Quantum Mechanics/Molecular Mechanics (QM/MM) Methods, each with its strengths and challenges.

4.2.1 Static water layer modeling

Static water layer modeling, where water molecules are arranged in pre-defined configurations around reactive sites, serves as a foundational approach to understand solvent effects in catalysis. The configuration of the water layer in static models typically relies on global optimization techniques or the deliberate organization of water molecules into well-defined structures, such as hexatomic rings.[54] These configurations aim to mimic the structured nature of water at interfaces or in confined spaces.[157] However, this structure has been reported to be a function of potential, as it was found that at more negative potentials the water became more disordered.[158] Interestingly, recent work has shown a break in the hydrogen binding network can improve the CO_2RR but hinder the HER.[159] Therefore, further work investigating the solvent's structural effects on the CO_2RR and c-CO_2RR is needed.

What has typically, been done to create an explicit solvent is to arrange one or two layers of water molecules around the reactive sites. Thus, researchers can investigate how the presence and specific arrangement of water molecules influence proton mobility and reaction pathways. This approach has provided valuable insights into the role of solvent structuring and hydrogen bonding networks in facilitating proton transfer. Nørskov and Chan *et al*. utilized one layer ice-like water along with H-down structure to model the electrochemical interface,[160] focusing on the proton transfer processes. The charge extrapolation method was used to achieve constant potential simulations.[135] This approach enabled them to elucidate the mechanisms underlying CO protonation, C-C coupling, the oxygen evolution reaction, and the hydrogen evolution reaction in detail. Similarly, Abild-Pedersen *et al*. applied this methodology to uncover the oxygenate/hydrocarbon selectivity for CO_2RR to C_2 products.[161]

To capture the characteristics of interfaces and simulate catalytic processes more accurately, a combination of a static water layer with a continuous solvent model was also adopted. Suntivich and Mavrikakis employed such hybrid method to quantify the potential of zero charge at the Pt-H2O electrochemical interface.[162] Wang *et al.* integrated two layers of water and implicit solvent model to predict the polarization curves for hydrogen evolution reaction.[163] However, the mixture of explicit water layer and implicit solvent will lead to unphysical invasion of continuum charges, a challenge highlighted in previous work.[144]

Moreover, the configuration of water molecules in static models significantly influences the identification and characterization of transition states in catalytic reactions. The presence and arrangement of water can stabilize or destabilize transition states, affecting the calculated activation energies. In addition, a fundamental critique of static water layer modeling is its inability to reflect the dynamics of water at the catalytic interface. Water molecules exhibit a high degree of mobility and can undergo rapid reorganization in response to changes in the reaction environment. This dynamic behavior plays a crucial role in solvent-mediated reactions, influencing the distribution of intermediates and transition states. Static models, by their nature, are unable to capture these dynamic processes, leading to a potential oversimplification of solvent effects in catalysis.

4.2.2 Molecular dynamics simulations

The limitations of static water layer modeling underscore the importance of incorporating more dynamic and flexible approaches, such as Molecular Dynamics (MD) simulations, to simulate solvent behavior more accurately. MD simulations can capture the constant motion and reorganization of water molecules, offering insights into the interfacial water structure. The structure of interfacial water molecules can significantly influence the adsorption, reaction kinetics, and overall efficiency of catalytic reactions. Through MD simulations, one can observe how water molecules orient themselves around catalysts and reactants, forming structured layers or disordered arrangements depending on the nature of the interface. This detailed view into the interfacial water structure helps in elucidating the role of hydration layers in affecting reaction barriers and mechanisms. Moreover, MD simulations allow for the explicit modeling of solvent molecules around adsorbates, capturing the dynamic solvent-adsorbate interactions that are often critical for understanding catalytic processes. For instance, solvent molecules can stabilize or destabilize certain reaction intermediates. Chan *et al*. employed MD simulations to evaluate the solvent energy of various intermediates in CO_2 reduction and oxygen redox reaction, like ∗CO, ∗CHO, ∗COH, ∗OCCHO, ∗OH, and ∗OOH on Cu, Au and Pt surfaces.[164] They concluded that the widely used continuum solvation models fall short in accurately representing solvent properties.

Enhanced sampling methods such as metadynamics and slow-growth techniques have been often integrated with MD simulations to explore the potential energy surface and to obtain the activation barrier of elementary steps. Wang *et al*. employed free energy integration method to explore the free energy surface of CO_2RR on FeN_4 single atom catalyst, where the electrode

potential was tuned by changing the ratio of Na+ and Cl–.[165] Hansen *et al*. utilized slow-growth sampling (SG-AIMD) method to explore the CO_2 reduction to CO on Au-water interfaces and they emphasized the crucial role of cation in facilitating CO_2 adsorption.[166] Goddard *et al*. applied the metadynamics technique to map out the free energy barriers for the elementary steps in CO_2RR on Cu(100) surfaces.[100] They discovered that under neutral conditions, CO_2 adsorption is the rate-limiting step in converting CO_2 to CO, with chemisorbed hydroxyl-methylene (CH−OH) emerging as the crucial intermediate that influences the selectivity towards methane production over methanol.

4.2.3 Quantum Mechanics/Molecular Mechanics (QM/MM) Methods

This hybrid computational technique effectively bridges the gap between the accurate, yet computationally intensive quantum mechanics (QM) methods and the less accurate, but more computationally efficient molecular mechanics (MM) methods. By doing so, QM/MM has emerged as a powerful tool for analyzing catalytic reactions in explicit solvent environments, offering a balanced compromise between computational feasibility and accuracy. It treats the catalytically active site and the immediate reaction environment using quantum mechanics, which provides a detailed and accurate description of electronic structures, bonding, and reactions. Concurrently, the bulk solvent and distant environment are modeled using molecular mechanics, which adequately captures the overall physical shape and properties of the system without the need for intensive computational resources. Explicit solvent modeling within the QM/MM framework allows for a detailed representation of solvent effects on catalytic reactions. By explicitly simulating solvent molecules around the reaction site using MM, researchers can investigate how solvent molecules influence reaction mechanisms, activation energies, and transition states. This approach is particularly useful for understanding solvation effects, solvent reorganization energy, and the dynamic interaction between the solvent and the reactants or catalysts. Steinmann *et al*. successfully developed a hybrid QM/MM method to model the adsorption behavior at metal/water interfaces.[153] They integrated the gas-phase adsorption free energies calculated at the DFT level with changes in solvation from the bulk phase to the interface, assessed through a MM-based alchemical transformation known as MMsolv. They evaluated the adsorption of a water molecule at the Pt/water interface, revealing our QM/MM hybrid scheme's intrinsic error is capped at 6 kcal mol−1 via a correction term, and demonstrate that the MMsolv solvation free energy of Pt closely aligns with experimental estimates. In addition, they calculated the adsorption energy of benzene and phenol at the Pt(111)/water interface, showing strong agreement with experiments that these aromatic molecules' adsorption is significantly less exothermic compared to a standard implicit solvent model, primarily due to competition with the solvent for adsorption sites on the metal surface, thus validating the hybrid QM/MM approach.

4.3 Functional Validation

It is important to discuss the accuracy benchmarking done for various functionals. Typically, in the c-CO_2RR, CO_2RR, and HER the common functionals used are PBE, RPBE, and

BEEF-vdW and for PBE and RPBE van der Waal corrections are introduced with Grimme's method[31,33,54,116,142,167–170] Wellendorff *et al*. explored the adsorption energy of various molecules (CO, H_2, CH_3OH, etc.) on various metals (Cu, Pt, Ni, etc.) The benchmarking was conducted against experimental results. In this work they compare LDA, PBE, PBESol, RPBE, PW91, and BEEF-vdW. They find that for systems that involve strong chemisorption, but little van der Waals contribution, RPBE and BEEF-vdW have mean absolute errors (MAE) less than 20 kJ/mol, PBE and PW91are slightly worse with MAE of about 25 kJ/mol, while PBESol and LDA perform much worse with MAEs of about 50 and 80 kJ/mol, respectively.[171]

To explore the effect of adding van der Waals corrections to the functional, Yuan *et al*. compared the adsorption of HCOOH and HCOO on Pt(111) experimentally against 14 different functionals. PBE and RPBE were found to perform terribly for HCOOH adsorption with adsorption energy differences of about 0.3 and 0.6 eV, respectively, from the experimental value. Surprisingly, BEEF-vdW, does not perform well on HCOOH (difference of about 0.2 eV), although given its large error of ± 0.222 eV, the edge of the error bar reaches near the experimental value.[172]

However, when adding van der Waals corrections we find that PBE does well. PBE-D3 is found to almost perfect match the experimental binding energy for HCOO and performs reasonably well for HCOOH. PBE-dDsC performs close to as well as PBE-D3. optPBE-vdW also performs very well for both binding energies. Given that HCOOH and HCOO adsorption on Pt(111) are chemically similar to the reactions that occur on the c-CO_2RR on metal surfaces we believe that PBE-D3, PBE-dDsC, and optPBE-vdW can perform well for c-CO_2RR systems.

5. Techniques used to model the reactivity of the c-CO_2RR, CO_2RR, and HER

In the context of electrochemical reactions, the onset potential is defined as the potential necessary for the reaction to start occurring. The overpotential is defined as the different between the onset potential and the equilibrium potential. In the case of the c-CO_2RR, there are three competing reactions (HER, CO_2RR, and c-CO_2RR). Thus, it is desirable to consider the onset potential of the various reactions as opposed to their overpotentials to allow for fair comparison.

It is noted that typically, the equilibrium potentials of the CO_2RR are less negative than the c-CO_2RR. However, it has been found that if proton source with a lower pK_a, such as NH_4^+, then the equilibrium potential of the c-CO_2RR becomes less negative than the CO_2RR.[31] However, regardless of proton source, the HER always has a less negative equilibrium potential than either the CO_2RR or the c-CO_2RR.

When examining reaction kinetics, another common tactic is to determine if a single elementary step is significantly kinetically slower than all the other steps. If this occurs, then it is possible to define the reactivity by this step. At this point no work has reported calculated activation barriers for the c-CO_2RR, and thus further work is needed in this area.

5.1 Reaction Pathway Analysis

Without kinetic data it can be challenging to determine a reaction pathway's reactivity. However, as these barriers are conducted under potential obtaining these barriers accurately is also difficult. Previous work assumed the kinetics were linked to the thermodynamics and that the potential limiting step was the most thermodynamically unfavorable step.[33] This is a computationally cheap method as it requires no explicit kinetic information, but it relies on the assumption that the thermodynamics are sufficient enough to provide the reactivity data. Previous work has shown that this does not necessarily hold for the CO_2RR.[160,173] Since no kinetics barriers for the c-CO_2RR have been published to this point it is unknown if the kinetics would be sufficiently described to the thermodynamics.

To compare the CO_2RR and the c-CO_2RR, Shen *et al*. compared the least exergonic step of the c-CO_2RR to the least exergonic step of the CO_2RR (CO_2 adsorption). They determine the potential limiting step of the c-CO_2RR to be the cleavage of the capture agent from the carbamate to form COOH*. Using this method, they determined that at weakly negative potentials the CO_2RR is more active than the NH_3 c-CO_2RR. However, they find a crossing at moderately negative potentials, and at highly negative potentials they predict that the c-CO_2RR is more active than the CO_2RR.[33]

Neves-Garcia *et al*. performed a similar analysis for the production of methane on both single atom alloy Ni on Au support (Ni@Au) as well as on pure Ni. They found that the free energy change to convert NH_2CO* to CO* on Ni@Au was 1.45 eV at 0 V vs. RHE or -0.47 V vs. SHE (pH = 8).[116] Although a direct comparison is difficult, as this value was not reported as a function of potential nor proton source, Shen *et al*. reported this value at -1.3 V vs. SHE and found on Ag(111) this free energy change to be about -0.6 eV.[33] Kowalski *et al*. reported that this reaction on Ag(111) was highly potential and proton source dependent. They found that when a H_2O proton source the free energy changes from about 1.5 eV to 0.4 eV as the potential changes from -1.0 V to -2.0 V vs. SHE. This range of reaction energies shifted to about 0.4 to -0.8 eV when an NH_4^+ proton source was used.[31] However, Neves-Garcia *et al*. finds that directly protonating the adsorbed NH_2CO* to form NH_2CHO* has a free energy change of -0.2 eV at 0 V vs. RHE (-0.47 V vs. SHE). Thus, they conclude because of the large thermodynamic barrier to produce CO and exergonic PCET to produce NH_2CHO*, the Ni@Au catalyst will be selective for CH_4.[116] Although not explicitly reported, as this step is a PCET, it is also likely highly potential and proton source dependent. Thus, it is likely that even at more reductive potentials, the PCET to convert NH_2CO* to NH_2CHO* is favored. They also compare their work on Ni@Au to a pure Ni surface at -0.83 V vs. SHE (-1.3 V vs. SHE). They find that each elementary pathway on Ni@Au is exergonic, while on Ni the final PCET to release the convert the NH_2* to NH_3 was slightly endergonic and thus, Ni requires a larger overpotential than Ni@Au.[116] However, the reaction in question is only uphill by about 0.2 eV, and thus for a more accurate comparison a more explicit kinetic analysis would be interesting to consider.

5.2 Energetic Span (ES)

As it was determined that there were multiple reasonable c-CO_2RR reaction pathways, using only the least favorable elementary step to describe the reactivity is risky as this decouples the different c-CO_2RR pathways. However, realistically, these pathways are not decoupled, but interact. Therefore, the energetic span (ES) theory provides a simple method to compare the reactivity of different pathways.

The ES method reported by Kozuch *et al*. defines the ES from Equation 22-23:[174,175]

$$ES = TS - I \quad \text{(if TS is after I)} \quad (22)$$

$$ES = TS - I + \Delta G_{rxn} \quad \text{(if TS is before I)} \quad (23)$$

In this method the ES of a pathway is defined as the largest energy difference between a transition state (TS) on the interesting pathway, and an intermediate (I) on any pathway. ΔG_{rxn} refers to the free energy of the overall reaction. To determine the ES, it is necessary to consider all possible spans from the all the TS along a given pathway against every intermediate. The largest of these spans is the ES. Figure 9 shows the ES on a cartoon reaction pathway.

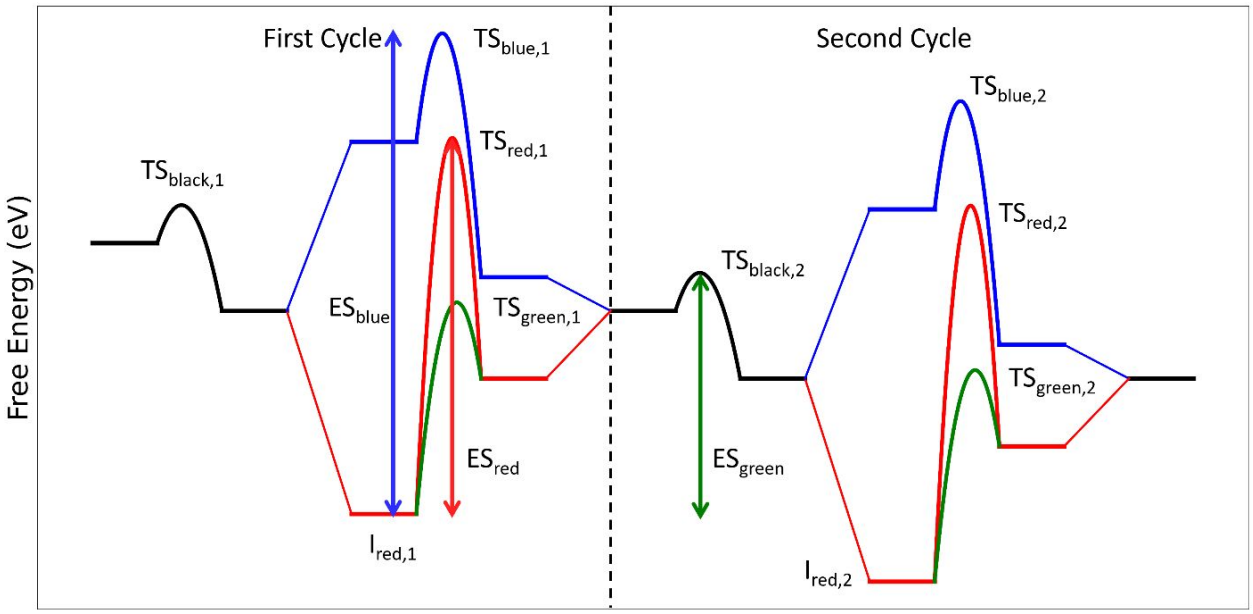

Figure 9: Cartoon pathway depicting the energetic span (ES) for two possible reaction pathways for various activation free energy values. These pathways assume that the barriers not shown are not rate determining. The arrow of a particular color represents the ES of that given pathway. Two complete cycles are shown. The red and green barriers are the kinetic barrier for the same reaction, but different values are used to show the effect of the magnitude of the barriers on the ES. The subscript shows the pathway and the cycle. The ES is not affected by which cycle it is computed on.

Some previous literatures have considered various c-CO_2RR reaction pathways.[31,116] Typically, if a pathway has a step that is too endergonic, it is considered to be inactive and not

considered in further kinetic simulations for simplicity. However, some work has shown that for the c-CO_2RR to CO various mechanisms are possible depending on the catalyst surface. Therefore, the reaction mechanism of the c-CO_2RR takes a similar shape to the cartoon shown in Figure 9. Both pathways start with identical intermediates, branch in the middle of the mechanism, and come together again to form the final product.

Figure 9 shows how to calculate the ES for the blue, red, and green pathways depending on the activation free energy barriers calculated. For the blue pathway shown the ES is simple. The most stable intermediate among any of the pathways is I_{red}. Then of the transition states on the blue pathway the one that would produce the largest ES with $I_{red,1}$ is $TS_{blue,1}$. $TS_{blue,1}$ occurs after $I_{red,1}$ so the ES is defined by $\mu_{TS_{blue,1}} - \mu_{I_{red,1}}$ (using Equation 22). For the red pathway the same logic can be applied. The most stable state is $I_{red,1}$ and the transition state along the red pathway that produces the largest ES is $TS_{red,1}$ so the ES is defined as $\mu_{TS_{red,1}} - \mu_{I_{red,1}}$ (using Equation 22). However, if the free energy of $TS_{red,1}$ was not given by the red curve, but instead by the green curve, then the ES would be defined by $\mu_{TS_{black,2}} - \mu_{I_{red,1}} = \mu_{TS_{black,1}} - \mu_{I_{red,1}} + \Delta\mu_{reaction}$ (using Equation 23). Thus, the green curve highlights the necessity to consider two consecutive cycles when using the ES method. If only one cycle was observed, it may appear that the ES for the green pathway was defined similar to the red pathways by $\mu_{TS_{green,1}} - \mu_{I_{red,1}}$. However, by including the second cycle it becomes clear that the kinetic barrier in the second cycle is relevant.

To this point, it was visually clear if a transition state occurred before or after an intermediate. However, it is imperative to define the terminology of before and after in the context of the c-CO_2RR. In the case of the c-CO_2RR, for a specific product all the pathways have the same generalized pathway. In the case of the production of CO, first the complex adsorbs. This is followed by three protonations and finished by the desorption of CO. Therefore, what was done in previous work was to assume intermediate that undergone the same number of each type of step were at the same point along the reaction pathway. For example, in the initial R-C cleavage pathway to reach the KCOOH* intermediate, one must adsorb $KRCO_2$, then undergo two protonations. For the final R-C cleavage pathway, if the adsorption and two protonations occur then the KRCO* intermediate is formed. Therefore, it is taken that KCOOH* and KRCO* are taken as being at the same point along their reaction pathways. As TS always occur in between intermediates this guarantees that a TS can be defined as before or after an intermediate of interest. However, when there are pathways that have different number of steps, then caution must be taken in using the ES and one must define what before and after mean between the reaction pathways with different number of steps.

Two important notes on the ES theory. It need not be necessary for the spans of all the different pathways to have the same most stable intermediate because of the definition of before and after. Also, the energetic span method is a simple approximation of the kinetics. It is far more desirable to conduct a full microkinetic model (MKM) as many works have done for the CO_2RR.[176,177] However, to our knowledge, a full MKM has yet to be developed for the c-CO_2RR.

From using the ES method, it has been reported that H_2O c-CO_2RR is thermodynamically easier than the NH_3 c-CO_2RR, assuming the same proton source is used.[31] This is likely because

of the difference in binding strength between the capture agent and the CO_2. From Zhang *et al*., it is predicted that NH_3 binds CO_2 stronger than H_2O does.[28] Therefore, as predicted from Appel *et al*. the overpotential for the H_2O c-CO_2RR is smaller than that of the NH_3 c-CO_2RR.[27]

It has also been shown that when $KHCO_3$ (pK_a of 10.3)[34] is used, the CO_2RR has a less negative onset potential than either c-CO_2RR reactions.[31] However, when NH_4^+ (pK_a of 9.25)[178] is used then the c-CO_2RR has a less negative onset potential than the CO_2RR. Therefore, further work needs to be done on exploring this proton source effect. Since the c-CO_2RR has one more protonation required than the CO_2RR the strength of the proton source has a larger effect on onset potential of the c-CO_2RR than the CO_2RR.

However, it has also been shown that the ammonium cation can have a detrimental effect on the selectivity. Since ammonium has a lower pK_a than $KHCO_3$ and H_2O (the typical CO_2RR proton sources), this means that the ammonium cation is more willing to release its proton. Therefore, it has been shown that when ammonium cations are present the HER dominates.[150] Thus, a balance occurs. The strong proton source is necessary to make the c-CO_2RR thermodynamically feasible, but the strong proton source also improves the HER. Therefore, further work must be done on finding catalysts and reaction conditions that severely hinder the HER, so that proton sources with lower pK_as can be used to conduct the c-CO_2RR.

5.3 Microkinetic Modeling (MKM)

To our knowledge most of the studies on the c-CO_2RR have used a thermodynamic analysis because of the lack of known kinetic barriers. In specific cases, the ES model has been used to obtain an effective barrier for a whole reaction pathway, and access the limiting potential, which is a kinetic related information. To our knowledge, more explicit kinetic simulations, as microkinetic modeling (MKM), have not been applied to c-CO_2RR, However, previous work has computed MKM for the CO_2RR and the HER. In this method, the complete thermodynamics and kinetics for the reaction are computed. A set of differential equations representing the rates of the elementary step is defined which must be solved together.[179] While solving the differential rate equations, the coverage of each intermediate is solved for simultaneously with the rates. This leads to being able to simulate the faradaic efficiency.[177] Therefore, MKM is a more complete calculations which allows for better comparison to experimental results.

MKM simulations for CO_2RR on Ag showed that when the solution is saturated with CO_2, at weakly negative potential the majority intermediate on the surface is COOH*. However, as the potential is made more negative, the surface get more covered in H* which leads to higher HER rates.[179]

Although out of the scope of this review, the c-CO_2RR is also heavily dependent on mass transport. Some previous works have combined results from MKM with transport base models to model the electrochemical reaction more effectively. This process involves using transport-based models to better approximate the concentrations of various molecules at the electrode. These concentrations are then fed into a MKM simulation. Singh *et al*. compared MKM of CO_2RR and HER on Ag with and without mass transfer effects. They were able to get similar experimental

current densities for the HER with and without the mass transfer effects, but mass transport effects were necessary to achieve similar results for the CO_2RR.[176]

6. Conclusions and Outlook

The goal of the c-CO_2RR is to directly reduce CO_2 in its captured state, avoiding the need for separate steps of capturing, compressing, releasing and then reducing the CO_2. Therefore, the capture agent that binds CO_2 the strongest may not be the best capture agent to conduct the c-CO_2RR. Most current research has focused on reducing amine captured CO_2 as amines are commonly used in industry as CO_2 capture agents. However, some research has started to branch out to other families of capture agents as well.

In the c-CO_2RR, three protonations are required, but there are only two free electrons per cycle, meaning that one protonation occurs via a chemical reaction. In this work we compared the reported mechanisms for the c-CO_2RR to form CO, formic acid and methane. All three works found that an additional protonation was necessary to convert the captured CO_2 into the desired product (three for CO and formic acid and nine for methane as compared to the two and eight PCETs needed to convert CO_2 into CO/formic acid and methane, respectively). As the field is new, there is limited research on how factors such as the effect capture agent, catalyst, and surface coverage impact the specific stage at which chemical protonation occurs.

It was shown that overall, with a proton source with a low enough pK_a, like NH_4ClO_4, the equilibrium potential for the reduction captured CO_2 into CO can be less negative than the reduction of free CO_2 into CO. However, for all proton sources tested, the equilibrium potential of the competitive HER was less negative than either the CO_2RR or the c-CO_2RR. Therefore, it is imperative to find a catalyst that severely hinders the HER either thermodynamically or kinetically enough so that the catalyst becomes selective for the CO_2RR or the c-CO_2RR.

To explore these electrochemical systems computationally, a variety of modeling techniques are available. The CHE method assumes that the only potential dependence is from the elementary electrochemical steps. However, in certain systems, including the c-CO_2RR, it is necessary to consider the potential dependence on the free energy of each of the intermediates. To adsorb the CO_2 onto the catalyst it has been shown that an electron transfer occurs. This is followed by a proton transfer to convert CO_2* into COOH*. This stepwise, decoupled proton-electron transfer contrasts with the CHE model, which requires all proton electron transfers to be coupled.

The surface charging method offers an alternative to more accurately model these more complex reactions. In this method the free energy is taken as a function of the potential, allowing for a more accurate description of the potential dependence of all reaction steps. This method relies on approximating the free energy as a second order Taylor Series as a function of the work function and capacitance. The work function can then be converted to electrode potential to get the free energy as a function of electrode potential.

As the CO_2RR and c-CO_2RR are typically conducted in solution phase, a method must be implemented to model the solvent and electrolyte. In this work we detail the methods used in the

VASPSol program, but the concepts can be extended to other computational frameworks as well. The solvent is modeled as a Polarizable Continuum Model (PCM) defined by the dielectric constant of the solvent instead of specific solvent molecules to significantly reduce the computational cost. The electrolyte is modeled as point charges by solving the linearized Poisson Boltzmann equation (LPBE) via the Debye Screening Length. The structures to be optimized are treated as solute and a cavity is formed in the PCM to place the solute. This method is computationally efficient, but difficulties such as solvent "leaking" into unphysical regions have been reported when using layers of solvent. Recently an updated framework called VASPSol++ has been released which adds volume to the solvent and electrolyte to prevent solvent leakage. Additionally, this framework can compute calculations at a given potential, while the traditional VASPSol method computes calculations at a given charge. Thus, VASPSol++ can significantly reduce the number of calculations necessary to obtain the free energy at a given potential. However, as this code is quite new further work needs to be done on benchmarking the computational cost as compared to VASPSol as well as how to properly define the additional parameters VASPSol++ requires.

However, there is room for improvement in regard to the modeling methods. As we reported explicit solvation is more accurate. Further work could explore the c-CO_2RR in more realistic explicit solvation models, which could assist in understanding better the role that the solvent and electrolyte have on facilitating the adsorption of the negatively charged reactant to the electrode surface.

As for the reactivity of the c-CO_2RR pathway, current work has mainly focused on approximating the kinetics via the thermodynamics. In some work, it has been assumed that the most endergonic step is the rate determining step, while other works use the energetic span model. Therefore, one of the main points that needs to be addressed in future work is to explicitly calculate kinetic barriers as have been done for the HER and CO_2RR in other works.[48,160] This will allow for more accurate kinetic simulations and more complex kinetic simulations could be conducted.

Unfortunately, at this point most computational results point to catalysts mainly being active towards the undesirable HER. However, to our knowledge, only metal catalysts have been explored for the c-CO2RR. There are other families of catalysts, such as metal-nitrogen doped graphite and molecular catalysts that are known to be selective for the CO_2RR.[180] Thus, further exploration into other catalysts families as well as looking for potential reaction descriptors are needed to better understand the c-CO2RR. Additionally, previous work has tried using aprotic solvents to further hinder the HER during the CO_2RR.[159] There has been some work on exploring other solvents in the c-CO2RR, namely alcohols. However, alcohols are chemically similar to water. Thus, future work can explore other types of solvents. It would be important to explore the solubility of these compound in those solvent since the reactant is a salt and not a neutral molecule like CO_2.

In general, the c-CO_2RR is a relatively new and promising reaction but remains underexplored. In this paper, we reviewed the reported mechanisms of the c-CO_2RR as well as methods employed in the literature to describe its reactivity. This work provides insight into computationally modeling the c-CO_2RR and highlights the complexities involved in these

calculations and providing guidance on improving these methods to further explore and understand the c-CO_2RR.

References

1 W. Cheng, L. Dan, X. Deng, J. Feng, Y. Wang, J. Peng, J. Tian, W. Qi, Z. Liu, X. Zheng, D. Zhou, S. Jiang, H. Zhao and X. Wang, *Sci. Data*, 2022, **9**, (83). DOI: 10.1038/s41597-022-01196-7.

2 F. C. García, E. Bestion, R. Warfield and G. Yvon-Durocher, *Proc. Natl. Acad Soc.*, 2018, **115** (43), 10989–10994.

3 J. T. Wootton, C. A. Pfister and J. D. Forester, *Proc. Natl. Acad. Soc.,* 2008, **105** (48), 18848–18853.

4 H. Coskun, A. Aljabour, P. De Luna, D. Farka, T. Greunz, D. Stifter, M. Kus, X. Zheng, M. Liu, A. W. Hassel, W. Schöfberger, E. H. Sargent, N. S. Sariciftci and P. Stadler, *Sci. Adv.*, 2017, **3**, (8). DOI: 10.1126/sciadv.1700686

5 Climate Change Atmospheric Carbon Dioxide, https://www.climate.gov/news-features/understanding-climate/climate-change-atmospheric-carbon-dioxide, (accessed April 2025).

6 A. Al-Mamoori, A. Krishnamurthy, A. A. Rownaghi and F. Rezaei, *Energy Technology*, 2017, **5** (6) DOI: 10.1002/ente.201600747.

7 D. Ravikumar, G. A. Keoleian, S. A. Miller and V. Sick, *Environ Sci Technol*, 2021, **55**, 12019–12031.

8 T. Zheng, K. Jiang and H. Wang, *Advanced Materials*, 2018, 30, (48), 1802066 DOI:10.1002/adma.201802066.

9 J. Wei, Q. Ge, R. Yao, Z. Wen, C. Fang, L. Guo, H. Xu and J. Sun, *Nat. Commun.*, 2017, **8**, 15174 DOI:10.1038/ncomms15174.

10 V. W. Y. Tam, A. Butera, K. N. Le and W. Li, *Construction and Building Materials*, 2020, **250** 118903, DOI: 10.1016/j.conbuildmat.2020.118903.

11 P. Ding, H. Zhao, T. Li, Y. Luo, G. Fan, G. Chen, S. Gao, X. Shi, S. Lu and X. Sun, *J. Mater. Chem. A,* 2020, **8**, 21947–21960.

12 S. Nitopi, E. Bertheussen, S. B. Scott, X. Liu, A. K. Engstfeld, S. Horch, B. Seger, I. E. L. Stephens, K. Chan, C. Hahn, J. K. Nørskov, T. F. Jaramillo and I. Chorkendorff, *Chemical Reviews*, 2019, **119** (12), 7610-7672.

13 D. Cheng, G. Zhang, L. Li, X. Shi, S. Zhen, Z. J. Zhao and J. Gong, *Chem Sci*, 2023, **14**, 7966–7972.

14 D. Cheng, Z. Wei, Z. Zhang, P. Broekmann, A. N. Alexandrova and P. Sautet, *Angewandte Chemie - International Edition*, **62** (20), DOI:10.1002/anie.202218575.

15 K. P. Kuhl, T. Hatsukade, E. R. Cave, D. N. Abram, J. Kibsgaard and T. F. Jaramillo, *J Am Chem Soc*, 2014, **136**, 14107–14113.

16 S. Kumari, A. N. Alexandrova and P. Sautet, *J Am Chem Soc*, 2023, **145**, 26350–26362.

17 A. K. Buckley, T. Cheng, M. H. Oh, G. M. Su, J. Garrison, S. W. Utan, C. Zhu, F. D. Toste, W. A. Goddard and F. M. Toma, *ACS Catal*, 2021, **11**, 9034–9042.

18 G. Marcandalli, A. Goyal and M. T. M. Koper, *ACS Catal*, 2021, **11**, 4936–4945.

19 Q. Zhu, J. Ma, X. Kang, X. Sun, H. Liu, J. Hu, Z. Liu and B. Han, *Angewandte Chemie*, 2016, **128**, 9158–9162.

20 B. Wulan, X. Cao, D. Tan, J. Ma and J. Zhang, *Adv Funct Mater*, 2023, **33** (1), 2209114, DOI:10.1002/adfm.202209114.

21 T. K. Todorova, M. W. Schreiber and M. Fontecave, *ACS Catal*, 2020, **10**, 1754–1768.

22 R. E. Siegel, S. Pattanayak and L. A. Berben, *ACS Catal*, 2023, **13**, 766–784.

23 J. Hack, N. Maeda and D. M. Meier, *ACS Omega*, 2022, **7** (44), 39520–39350.

24 T. Davran-Candan, *Journal of Physical Chemistry A*, 2014, **118**, 4582–4590.

25 B. Arstad, H. Fjellvåg, K. O. Kongshaug, O. Swang and R. Blom, *Adsorption*, 2008, **14**, 755–762.

26 M. Afkhamipour and M. Mofarahi, *RSC Adv.*, 2017, **7**, 17857–17872.

27 A. M. Appel and J. Y. Yang, *ACS Energy Letters*, 2024, **9** (2), 768–770.

28 Z. Zhang, A. L. Kummeth, J. Y. Yang and A. N. Alexandrova, *Proc. Natl. Acad. Sci.*, 2022, **119** (25), e2123496119, DOI: 10.1073/pnas.2123496119.

29 G. Lee, Y. C. Li, J. Y. Kim, T. Peng, D. H. Nam, A. Sedighian Rasouli, F. Li, M. Luo, A. H. Ip, Y. C. Joo and E. H. Sargent, *Nat Energy*, 2021, **6**, 46–53.

30 G. Lee, A. S. Rasouli, B. H. Lee, J. Zhang, D. H. Won, Y. C. Xiao, J. P. Edwards, M. G. Lee, E. D. Jung, F. Arabyarmohammadi, H. Liu, I. Grigioni, J. Abed, T. Alkayyali, S. Liu, K. Xie, R. K. Miao, S. Park, R. Dorakhan, Y. Zhao, C. P. O'Brien, Z. Chen, D. Sinton and E. Sargent, *Joule*, 2023, **7**, 1277–1288.

31 R. M. Kowalski, A. Banerjee, C. Yue, S. G. Gracia, D. Cheng, C. G. Morales-Guio and P. Sautet, *J. Am. Chem. Soc.*, 2024, **146** (30), 20728–20741.

32 H. Ma, E. Ibáñez-Alé, R. Ganganahalli, J. Pérez-Ramírez, N. López and B. S. Yeo, *J. Am. Chem. Soc.*, 2023, **145** (45), 24707–24716.

33 K. Shen, D. Cheng, E. Reyes-Lopez, J. Jang, P. Sautet and C. G. Morales-Guio, *Joule*, 2023, **7**, 1260–1276.

34 G. Leverick, E. M. Bernhardt, A. I. Ismail, J. H. Law, A. Arifutzzaman, M. K. Aroua and B. M. Gallant, *ACS Catal*, 2023, **13**, 12322–12337.

35 Z. Zhang, H. Li, Y. Shao, L. Gan, F. Kang, W. Duan, H. A. Hansen and J. Li, *Nat. Commun.*,2024, **15** 612, DOI:10.1038/s41467-024-44896-x.

36 X. Qin, H. A. Hansen, K. Honkala and M. M. Melander, *Nat. Commun.*, 2023, **14**, 7607, DOI:10.1038/s41467-023-43300-4.

37 D. D. Bodé Jr., T. N. Andersen and H. Eyring, *J. Electrochem. Soc.*, 1967, **114** (72), DOI: 10.1149/1.2426510

38 N. Mohandas, S. Bawari, J. J. T. Shibuya, S. Ghosh, J. Mondal, T. N. Narayanan and A. Cuesta, *Chem. Sci.*, 2024, **15**, 6643–6660.

39 S. J. Shin, H. Choi, S. Ringe, D. H. Won, H. S. Oh, D. H. Kim, T. Lee, D. H. Nam, H. Kim and C. H. Choi, *Nat. Commun.*, 2022, **13**, 5482 DOI:10.1038/s41467-022-33199-8.

40 L. I. Bendavid and E. A. Carter, *Journal of Physical Chemistry C*, 2013, **117**, 26048–26059.

41 J. Shen, M. J. Kolb, A. J. Göttle and M. T. M. Koper, *Journal of Physical Chemistry C*, 2016, **120**, 15714–15721.

42 J. Wu, W. Li, K. Liu, A. Kucernak, H. Liu, L. Chai and M. Liu, *Next Energy*, 2023, **1**, 100032, DOI:10.1016/j.nxener.2023.100032.

43 J. Wu, Y. Huang, W. Ye and Y. Li, *Advanced Science*, 2017, **4** (11), 1700194, DOI: 10.1002/advs.201700194.

44 T. Cheng, H. Xiao and W. A. Goddard, *J Am Chem Soc*, 2016, **138**, 13802–13805.

45 S. Liang, L. Huang, Y. Gao, Q. Wang and B. Liu, *Advanced Science*, 2021, **8** (24), 2102886, DOI: 10.1002/advs.202102886.

46 G. Marcandalli, M. C. O. Monteiro, A. Goyal and M. T. M. Koper, *Acc Chem Res*, 2022, **55**, 1900–1911.

47 Y. A. Alsunni, A. W. Alherz and C. B. Musgrave, *Journal of Physical Chemistry C*, 2021, **125**, 23773–23783.

48 D. Bohra, I. Ledezma-Yanez, G. Li, W. de Jong, E. A. Pidko and W. A. Smith, *Angewandte Chemie - International Edition*, 2019, **58**, 1345–1349.

49 X. Wang, D. Toroz, S. Kim, S. L. Clegg, G. S. Park and D. Di Tommaso, *Physical Chemistry Chemical Physics*, 2020, **22**, 16301–16313.

50 T. T. Duignan, C. J. Mundy, G. K. Schenter and X. S. Zhao, *J. Chem. Theory Comput.*, 2020, **16**, 5401–5409.

51 N. Karmodak, S. Vijay, G. Kastlunger and K. Chan, *ACS Catal.*, 2022, **12**, 4818–4824.

52 S. Vijay, W. Ju, S. Brückner, S. C. Tsang, P. Strasser and K. Chan, *Nat. Catal.*, 2021, **4**, 1024–1031.

53 A. Rendón-Calle, S. Builes and F. Calle-Vallejo, *Current Opinion in Electrochemistry.*, 2018, **9**, 158-165, DOI: 10.1016/j.coelec.2018.03.012.

54 M. T. Tang, X. Liu, Y. Ji, J. K. Norskov and K. Chan, *Journal of Physical Chemistry C*, 2020, **124**, 28083–28092.

55 R. Kortlever, J. Shen, K. J. P. Schouten, F. Calle-Vallejo and M. T. M. Koper, *Journal of Physical Chemistry Letters*, 2015, **6**, 4073–4082.

56 Q. Cheng, M. Huang, Q. Ye, B. Deng and F. Dong, *Chinese Chemical Letters.*, 2024, **35** (6), 109112, DOI: 10.1016/j.cclet.2023.109112.

57 A. Zhang, Y. Liang, H. Li, B. Zhang, Z. Liu, Q. Chang, H. Zhang, C. F. Zhu, Z. Geng, W. Zhu and J. Zeng, *Nano. Lett.*, 2020, **20**, 8229–8235.

58 W. Ma, S. Xie, X. G. Zhang, F. Sun, J. Kang, Z. Jiang, Q. Zhang, D. Y. Wu and Y. Wang, *Nat. Commun.*, **10**, 892, DOI:10.1038/s41467-019-08805-x.

59 Z. Liu, C. Liu, S. Mao and X. Huang, *ACS Appl. Mater. Interfaces*, 2023, **15**, 7529–7537.

60 J. T. Feaster, C. Shi, E. R. Cave, T. Hatsukade, D. N. Abram, K. P. Kuhl, C. Hahn, J. K. Nørskov and T. F. Jaramillo, *ACS Catal.*, 2017, **7**, 4822–4827.

61 J. Lim, P. W. Kang, S. S. Jeon and H. Lee, *J. Mater. Chem. A Mater.*, 2020, **8**, 9032–9038.

62 H. Ji Jang, J. Hyun Yang, J. Young Maeng, Y. Jun Kim, C. Kyun Rhee and Y. Sohn, *Appl. Surf. Sci.* 2022, **604**, 154438, DOI:10.1016/j.apsusc.2022.154438.

63 S. Y. Choi, S. K. Jeong, H. J. Kim, I. H. Baek and K. T. Park, *ACS Sustain Chem. Eng.*, 2016, **4**, 1311–1318.

64 B. Eneau-Innocent, D. Pasquier, F. Ropital, J. M. Léger and K. B. Kokoh, *Appl. Catal. B*, 2010, **98**, 65–71.

65 B. Innocent, D. Liaigre, D. Pasquier, F. Ropital, J. M. Léger and K. B. Kokoh, *J. Appl. Electrochem.*, 2009, **39**, 227–232.

66 F. Yang, A. O. Elnabawy, R. Schimmenti, P. Song, J. Wang, Z. Peng, S. Yao, R. Deng, S. Song, Y. Lin, M. Mavrikakis and W. Xu, *Nat. Commun.*, **11**, 1088, DOI:10.1038/s41467-020-14914-9.

67 W. Du, M. Li, Q. Liu and R. Chen, *New Journal of Chemistry*, 2024, **48**, 6000–6008, DOI:10.1039/d3nj05873e.

68 D. Tan, W. Lee, Y. E. Kim, Y. N. Ko, M. H. Youn, Y. E. Jeon, J. Hong, J. E. Park, J. Seo, S. K. Jeong, Y. Choi, H. Choi, H. Y. Kim and K. T. Park, *ACS Appl. Mater. Interfaces*, 2022, **14**, 28890–28899.

69 W. Chen, Y. Wang, Y. Li and C. Li, *Chinese Chemical Society*, 2023, **5**, 544–567.

70 X. Du Liang, N. Tian, S. N. Hu, Z. Y. Zhou and S. G. Sun, *Materials Report: Energy,* 2023, **3** (2), 100191, DOI: 10.1016/j.matre.2023.100191.

71 Z. Li, Y. Yang, H. Ding, Z. Li, L. Wang, X. Zhang, J. Li, W. Xie, X. Hu, B. Wang and M. Wei, *Chem. Catalysis*, **3** (10), 100767, DOI:10.1016/j.checat.2023.100767.

72 N. B. D. Monti, M. Fontana, A. Sacco, A. Chiodoni, A. Lamberti, C. F. Pirri and J. Zeng, *ACS Appl. Energy Mater.*, 2022, **5**, 14779–14788.

73 S. Liu, C. Sun, J. Xiao and J. L. Luo, *ACS Catal.*, 2020, **10**, 3158–3163.

74 W. Sheng, M. Myint, J. G. Chen and Y. Yan, *Energy Environ. Sci.*, 2013, **6**, 1509–1512.

75 A. R. Woldu, Z. Huang, P. Zhao, L. Hu and D. Astruc, *Coordination Chemistry* Reviews, 2022, **454**, 214340, DOI: 10.1016/j.ccr.2021.214340.

76 Q. Chang, J. H. Lee, Y. Liu, Z. Xie, S. Hwang, N. S. Marinkovic, A. H. A. Park, S. Kattel and J. G. Chen, *JACS Au*, 2022, **2**, 214–222.

77 Q. Kong, X. An, Q. Liu, L. Xie, J. Zhang, Q. Li, W. Yao, A. Yu, Y. Jiao and C. Sun, *Royal Society of Chemistry*, 2023, *Mater. Horiz.*, **10**, 698–721.

78 Y. Guan, J. Kümper, S. D. Mürtz, S. Kumari, P. J. C. Hausoul, R. Palkovits and P. Sautet, *Chem. Sci.*, 2024, **15**, 14485–14496.

79 J. Choi, S. Chiu, A. Banerjee, R. L. Sacci, G. M. Veith, C. Stieber, C. Hahn, A. N. Alexandrova and C. G. Morales-Guio, *Journal of Physical Chemistry Letters*, 2024, **15**, 8007–8017.

80 Y. Hori, *Modern Aspects of Electrochemistry*, vol: 42, C. G. Vayenas, Springer, New York, NY, 2008 Chapter 3, *Electrochemical CO 2 Reduction on Metal Electrodes*, 89-189.

81 T. E. Teeter and P. Van Rysselberghe, *The Journal of Chemical Physics*, 1954, **22**, 759–760.

82 A. Bagger, W. Ju, A. S. Varela, P. Strasser and J. Rossmeisl, *ChemPhysChem*, 2017, **18**, 3266–3273.

83 H. Pan and C. J. Barile, *Energy Environ. Sci.*, 2020, **13**, 3567–3578.

84 J. Cai, Q. Zhao, W. Y. Hsu, C. Choi, Y. Liu, J. M. P. Martirez, C. Chen, J. Huang, E. A. Carter and Y. Huang, *J. Am. Chem. Soc*, 2023, **145**, 9136–9143.

85 C. A. Obasanjo, G. Gao, J. Crane, V. Golovanova, F. P. García de Arquer and C. T. Dinh, *Nat. Commun.*, 2023, 14, 3176, DOI:10.1038/s41467-023-38963-y.

86 J. Zhang, G. Zeng, S. Zhu, H. Tao, Y. Pan, W. Lai, J. Bao, C. Lian, D. Su, M. Shao and H. Huang, *Proc. Natl. Acad. Sci.*, DOI:10.1073/pnas.2218987120.

87 X. Wei, Z. Yin, K. Lyu, Z. Li, J. Gong, G. Wang, L. Xiao, J. Lu and L. Zhuang, *ACS Catal.*, 2020, **10**, 4103–4111.

88 Q. Zhu, X. Sun, D. Yang, J. Ma, X. Kang, L. Zheng, J. Zhang, Z. Wu and B. Han, *Nat. Commun.*, 2019, **10**, 3851, DOI:10.1038/s41467-019-11599-7.

89 X. Liu, P. Schlexer, J. Xiao, Y. Ji, L. Wang, R. B. Sandberg, M. Tang, K. S. Brown, H. Peng, S. Ringe, C. Hahn, T. F. Jaramillo, J. K. Nørskov and K. Chan, *Nat. Commun.*, 2019, **10**, 32 DOI:10.1038/s41467-018-07970-9.

90 E. Pérez-Gallent, M. C. Figueiredo, F. Calle-Vallejo and M. T. M. Koper, *Angewandte Chemie*, 2017, **129**, 3675–3678.

91 Y. Hori, R. Takahashi, Y. Yoshinami and A. Murata, *J. Phys. Chem. B*, 1997, **101** (36), 7075–7081.

92 J. H. Montoya, A. A. Peterson and J. K. Nørskov, *ChemCatChem*, 2013, **5**, 737–742.

93 D. Cheng, A. N. Alexandrova and P. Sautet, *Journal of Physical Chemistry Letters*, 2024, **15**, 1056–1061.

94 X. Chang, J. Li, H. Xiong, H. Zhang, Y. Xu, H. Xiao, Q. Lu and B. Xu, *Angewandte Chemie - International Edition*, 2022, **61** (2), e202111167, DOI:10.1002/anie.202111167.

95 W. Deng, P. Zhang, Y. Qiao, G. Kastlunger, N. Govindarajan, A. Xu, I. Chorkendorff, B. Seger and J. Gong, *Nat. Commun.*, 2024, **15** (892), DOI:10.1038/s41467-024-45230-1.

96 J. H. Montoya, C. Shi, K. Chan and J. K. Nørskov, *Journal of Physical Chemistry Letters*, 2015, **6**, 2032–2037.

97 H. Peng, M. T. Tang, X. Liu, P. Schlexer Lamoureux, M. Bajdich and F. Abild-Pedersen, *Energy Environ. Sci.*, 2021, **14**, 473–482.

98 J. D. Goodpaster, A. T. Bell and M. Head-Gordon, *Journal of Physical Chemistry Letters*, 2016, **7**, 1471–1477.

99 T. Cheng, H. Xiao and W. A. Goddard, *Journal of Physical Chemistry Letters*, 2015, **6**, 4767–4773.

100 T. Cheng, H. Xiao and W. A. Goddard, *Pro.c Natl. Acad. Sci*, 2017, **114**, 1795–1800.

101 Y. Hori, H. Wakebe, T. Tsukamoto and O. Koga, *Surface* Science, 1995, **335**, 258–263.

102 C. Hahn, T. Hatsukade, Y. G. Kim, A. Vailionis, J. H. Baricuatro, D. C. Higgins, S. A. Nitopi, M. P. Soriaga and T. F. Jaramillo, *Proc. Natl. Acad. Sci.*, 2017, **114**, 5918–5923.

103 D. Cheng, Z. J. Zhao, G. Zhang, P. Yang, L. Li, H. Gao, S. Liu, X. Chang, S. Chen, T. Wang, G. A. Ozin, Z. Liu and J. Gong, *Nat. Commun.*, 2021, 12, 395, DOI:10.1038/s41467-020-20615-0.

104 D. Cheng, G. Zhang, L. Li, X. Shi, S. Zhen, Z. J. Zhao and J. Gong, *Chem Sci*, 2023, **14**, 7966–7972.

105 F. Scholten, K. L. C. Nguyen, J. P. Bruce, M. Heyde and B. Roldan Cuenya, *Angewandte Chemie - International Edition*, 2021, **60**, 19169–19175.

106 D. Cheng, K.-L. C. Nguyen, V. Sumaria, Z. Wei, Z. Zhang, W. Gee, Y. Li, C. G. Morales-Guio, M. Heyde, B. Roldan Cuenya, A. N. Alexandrova and P. Sautet, *ChemrRxiv*, 2024 DOI:10.26434/chemrxiv-2024-z3dlp-v2.

107 F. Calle-Vallejo and M. T. M. Koper, *Angewandte Chemie - International Edition*, 2013, **52**, 7282–7285.

108 K. J. P. Schouten, E. Pérez Gallent and M. T. M. Koper, *ACS Catal.*, 2013, **3**, 1292–1295.

109 T. T. Zhuang, Z. Q. Liang, A. Seifitokaldani, Y. Li, P. De Luna, T. Burdyny, F. Che, F. Meng, Y. Min, R. Quintero-Bermudez, C. T. Dinh, Y. Pang, M. Zhong, B. Zhang, J. Li, P. N. Chen, X. L. Zheng, H. Liang, W. N. Ge, B. J. Ye, D. Sinton, S. H. Yu and E. H. Sargent, *Nat. Catal.*, 2018, **1**, 421–428.

110 Z. Li, P. Wang, X. Lyu, V. K. R. Kondapalli, S. Xiang, J. D. Jimenez, L. Ma, T. Ito, T. Zhang, J. Raj, Y. Fang, Y. Bai, J. Li, A. Serov, V. Shanov, A. I. Frenkel, S. D. Senanayake, S. Yang, T. P. Senftle and J. Wu, *Nature Chemical Engineering*, 2024, **1**, 159–169.

111 D. Cheng, G. Zhang, L. Li, X. Shi, W. Zhu, X. Yuan, L. Moskaleva, P. Zhang, Z. J. Zhao and J. Gong, *Sci. China Chem.*, 2024, **68**, 763–771.

112 E. Bertheussen, A. Verdaguer-Casadevall, D. Ravasio, J. H. Montoya, D. B. Trimarco, C. Roy, S. Meier, J. Wendland, J. K. Nørskov, I. E. L. Stephens and I. Chorkendorff, *Angewandte Chemie*, 2016, **128**, 1472–1476.

113 Y. Lum, T. Cheng, W. A. Goddard and J. W. Ager, *J. Am. Chem. Soc.*, 2018, **140**, 9337–9340.

114 E. L. Clark, J. Wong, A. J. Garza, Z. Lin, M. Head-Gordon and A. T. Bell, *J. Am. Chem. Soc.*, 2019, **141**, 4191–4193.

115 K. Chan, *Nat. Commum.*, 2020, **11**, 5954, DOI: 10.1038/s41467-020-19369-6.

116 T. Neves-Garcia, M. Hasan, Q. Zhu, J. Li, Z. Jiang, Y. Liang, H. Wang, L. M. Rossi, R. E. Warburton and L. R. Baker, *J. Am. Chem. Soc.*, 2024, **146** (46), 31633–31646.

117 Z. T. Wang, M. T. Darby, A. J. Therrien, M. El-Soda, A. Michaelides, M. Stamatakis and E. C. H. Sykes, *Journal of Physical Chemistry C*, 2016, **120**, 13574–13580.

118 F. Bao, E. Kemppainen, I. Dorbandt, R. Bors, F. Xi, R. Schlatmann, R. van de Krol and S. Calnan, *ChemElectroChem*, 2021, **8**, 195–208.

119 J. K. Nørskov, J. Rossmeisl, A. Logadottir, L. Lindqvist, J. R. Kitchin, T. Bligaard and H. Jónsson, *Journal of Physical Chemistry B*, 2004, **108**, 17886–17892.

120 X. Zhang and Z. Zhou, *Journal of Physical Chemistry C*, 2022, **126**, 3820–3829.

121 J. C. Fornaciari, L. C. Weng, S. M. Alia, C. Zhan, T. A. Pham, A. T. Bell, T. Ogitsu, N. Danilovic and A. Z. Weber, *Electrochim. Act.*, 2022, **405**, 139810, DOI:10.1016/j.electacta.2021.139810.

122 A. S. Varela, *Current opinion in Green and Sustainable Chemistry*, 2020, **26**, 100371, DOI: 10.1016/j.cogsc.2020.100371.

123 T. P. Silverstein and S. T. Heller, *J. Chem. Educ.*, 2017, **94**, 690–695.

124 N. Oppel, P. Röse, S. Heuser, M. Prokein, U. P. Apfel and U. Krewer, *Electrochim. Acta*, 2024, **490**, 144270, DOI:10.1016/j.electacta.2024.144270.

125 J. A. Gauthier, C. F. Dickens, H. H. Heenen, S. Vijay, S. Ringe and K. Chan, *J. Chem. Theory Comput.*, 2019, **15**, 6895–6906.

126 R. E. Warburton, A. V. Soudackov and S. Hammes-Schiffer, *Chem. Rev.*, 2022, **122** (12), 10599–10650.

127 Sergio Transatti, *Journal of Electroanalytical Chemistry and Interfacial Electrochemistry*, 1986, **209** (2), 417–428.

128 A. A. Isse and A. Gennaro, *Journal of Physical Chemistry B*, 2010, **114**, 7894–7899.

129 S. N. Steinmann, C. Michel, R. Schwiedernoch, J. S. Filhol and P. Sautet, *ChemPhysChem*, 2015, **16**, 2307–2311.

130 M. A. Ramzan, R. Favre, S. N. Steinmann, T. Le Bahers and P. Raybaud, *Journal of Physical Chemistry C*, 2024, **128**, 10025–10034.

131 H. Cao, Z. Zhang, J. W. Chen and Y. G. Wang, *ACS Catal.*, 2022, **12**, 6606–6617.

132 J. A. Gauthier, C. F. Dickens, H. H. Heenen, S. Vijay, S. Ringe and K. Chan, *J. Chem. Theory Comput.*, 2019, **15**, 6895–6906.

133 S. M. R. Islam, F. Khezeli, S. Ringe and C. Plaisance, *Journal of Chemical Physics*, 2023, **159** (23), 234117, DOI:10.1063/5.0176308.

134 R. Sundararaman, K. Letchworth-Weaver, K. A. Schwarz, D. Gunceler, Y. Ozhabes and T. A. Arias, *SoftwareX*, 2017, **6**, 278–284.

135 K. Chan and J. K. Nørskov, *Journal of Physical Chemistry Letters*, 2015, **6**, 2663–2668.

136 K. Mathew, R. Sundararaman, K. Letchworth-Weaver, T. A. Arias and R. G. Hennig, *Journal of Chemical Physics*, 2014, **140** (8), 084106, DOI:10.1063/1.4865107.

137 K. Mathew, V. S. C. Kolluru, S. Mula, S. N. Steinmann and R. G. Hennig, *Journal of Chemical Physics*, 2019, **151** (23), 234101, DOI:10.1063/1.5132354.

138 J. Mähler and I. Persson, *Inorg Chem*, 2012, **51**, 425–438.

139 I. Persson, *Dalton Transactions*, 2024, **53**, 15517–15538.

140 S. N. Steinmann and P. Sautet, *Journal of Physical Chemistry C*, 2016, **120**, 5619–5623.

141 G. Kresse and J. Furthmüller, *Phys. Rev. B*, 1996, **54**, 11169, 169–186.

142 G. Kresse and J. Furthmüller, *Computational Materials Science*, 1996, **6** (1), 15-50.

143 S. Kumari and P. Sautet, *Journal of Physical Chemistry Letters*, 2023, **14**, 2635–2643.

144 J. A. Gauthier, S. Ringe, C. F. Dickens, A. J. Garza, A. T. Bell, M. Head-Gordon, J. K. Nørskov and K. Chan, *ACS Catal.*, 2019, **9**, 920–931.

145 J. A. Gauthier, C. F. Dickens, S. Ringe and K. Chan, *ChemPhysChem*, 2019, **20**, 3074–3080.

146 R. Sundararaman and W. A. Goddard, *Journal of Chemical Physics*, 2015, **142** (6), 064107, DOI:10.1063/1.4907731.

147 R. Sundararaman, K. A. Schwarz, K. Letchworth-Weaver and T. A. Arias, *Journal of Chemical Physics*, 2015, **142** (5), 054102, DOI:10.1063/1.4906828.

148 M. Van Den Bossche, E. Skúlason, C. Rose-Petruck and H. Jónsson, *Journal of Physical Chemistry C*, 2019, **123**, 4116–4124.

149 D. Henderson and D. Boda, *Physical Chemistry Chemical Physics*, 2009, **11**, 3822–3830.

150 J. Safipour, A. Z. Weber and A. T. Bell, *ACS Energy Lett.*, 2023, **8**, 5012–5017.

151 D. A. Case, H. M. Aktulga, K. Belfon, D. S. Cerutti, G. A. Cisneros, V. W. D. Cruzeiro, N. Forouzesh, T. J. Giese, A. W. Götz, H. Gohlke, S. Izadi, K. Kasavajhala, M. C. Kaymak, E. King, T. Kurtzman, T. S. Lee, P. Li, J. Liu, T. Luchko, R. Luo, M. Manathunga, M. R. Machado, H. M. Nguyen, K. A. O'Hearn, A. V. Onufriev, F. Pan, S. Pantano, R. Qi, A. Rahnamoun, A. Risheh, S. Schott-Verdugo, A. Shajan, J. Swails, J. Wang, H. Wei, X. Wu, Y. Wu, S. Zhang, S. Zhao, Q. Zhu, T. E. Cheatham, D. R. Roe, A. Roitberg, C. Simmerling, D. M. York, M. C. Nagan and K. M. Merz, *J Chem Inf Model*, 2023, **63**, 6183–6191.

152 D.A. Case, H.M. Aktulga, K. Belfon, I.Y. Ben-Shalom, J.T. Berryman, S.R. Brozell, D.S. Cerutti, T.E. Cheatham, III, G.A. Cisneros, V.W.D. Cruzeiro, T.A. Darden, N. Forouzesh, M. Ghazimirsaeed, G. Giambaşu, T. Giese, M.K. Gilson, H. Gohlke, A.W. Goetz, J.

Harris, Z. Huang, S. Izadi, S.A. Izmailov, K. Kasavajhala, M.C. Kaymak, A. Kovalenko, T. Kurtzman, T.S. Lee, P. Li, Z. Li, C. Lin, J. Liu, T. Luchko, R. Luo, M. Machado, M. Manathunga, K.M. Merz, Y. Miao, O. Mikhailovskii, G. Monard, H. Nguyen, K.A. O'Hearn, A. Onufriev, F. Pan, S. Pantano, A. Rahnamoun, D.R. Roe, A. Roitberg, C. Sagui, S. Schott-Verdugo, A. Shajan, J. Shen, C.L. Simmerling, N.R. Skrynnikov, J. Smith, J. Swails, R.C. Walker, J. Wang, J. Wang, X. Wu, Y. Wu, Y. Xiong, Y. Xue, D.M. York, C. Zhao, Q. Zhu, and P.A. Kollman (2024), Amber 2024, University of California, San Francisco.

153 P. Clabaut, B. Schweitzer, A. W. Götz, C. Michel and S. N. Steinmann, *J. Chem. Theory Comput.*, 2020, **16**, 6539–6549.

154 S. N. Steinmann, R. Ferreira De Morais, A. W. Götz, P. Fleurat-Lessard, M. Iannuzzi, P. Sautet and C. Michel, *J. Chem. Theory Comput.*, 2018, **14**, 3238–3251.

155 P. Clabaut, M. Beisert, C. Michel and S. N. Steinmann, *Journal of Chemical Physics*, 2022, **157** (19), 194705, DOI:10.1063/5.0130368.

156 Y. Guan, J. Kümper, S. Kumari, N. Heiming, S. D. Mürtz, S. N. Steinmann, S. Palkovits, R. Palkovits and P. Sautet, *ACS Appl. Mater. Interfaces*, 2025, **17**, 4087–4097.

157 S. Chakraborty, H. Kumar, C. Dasgupta and P. K. Maiti, *Acc. Chem. Res.*, 2017, **50**, 2139–2146.

158 J.-J. Velasco-Velez, C. H. Wu, T. A. Pascal, L. F. Wan, J. Guo, D. Prendergast and M. Salmeron, *Science*, 2014, **346** (6211), 831–834.

159 R. J. Gomes, R. Kumar, H. Fejzić, B. Sarkar, I. Roy and C. V. Amanchukwu, *Nat. Catal.*, 2024, **7**, 689–701.

160 X. Liu, J. Xiao, H. Peng, X. Hong, K. Chan and J. K. Nørskov, *Nat. Commun.*, 2017, **8**, 15438, DOI:10.1038/ncomms15438.

161 H. J. Peng, M. T. Tang, J. Halldin Stenlid, X. Liu and F. Abild-Pedersen*, Nat. Commun.*, 2022, **13**, 1399, DOI:10.1038/s41467-022-29140-8.

162 P. Xu, A. D. von Rueden, R. Schimmenti, M. Mavrikakis and J. Suntivich, *Nat Mater*, 2023, **22**, 503–510.

163 G. Gao and L. W. Wang, *Chem Catalysis*, 2021, **1**, 1331–1345.

164 H. H. Heenen, J. A. Gauthier, H. H. Kristoffersen, T. Ludwig and K. Chan, *Journal of Chemical Physics*, 2020, **152** (14), 144703, DOI:10.1063/1.5144912.

165 H. Zhao, H. Cao, Z. Zhang and Y. G. Wang, *ACS Catal*, 2022, **12**, 11380–11390.

166 X. Qin, T. Vegge and H. A. Hansen, *ACS Catal.*, 2024, **14**, 8168–8175.

167 J. H. Montoya, C. Shi, K. Chan and J. K. Nørskov, *Journal of Physical Chemistry Letters*, 2015, **6**, 2032–2037.

168 S. Grimme, J. Antony, S. Ehrlich and H. Krieg, *Journal of Chemical Physics*, 2010, **132** (15),154104, DOI:10.1063/1.3382344.

169 B. Hammer, L. B. Hansen and J. K. Nørskov, *Phys. Rev. B*, 1999, **59**, 7413, DOI: 10.1103/PhysRevB.59.7413.

170 J. Wellendorff, K. T. Lundgaard, A. Møgelhøj, V. Petzold, D. D. Landis, J. K. Nørskov, T. Bligaard and K. W. Jacobsen, *Phys Rev B*, 2012, **85**, 235149, DOI:10.1103/PhysRevB.85.235149.

171 J. Wellendorff, T. L. Silbaugh, D. Garcia-Pintos, J. K. Nørskov, T. Bligaard, F. Studt and C. T. Campbell, *Surf Sci*, 2015, **640**, 36–44.

172 D. Yuan, H. Liao and W. Hu, *Physical Chemistry Chemical Physics*, 2019, **21**, 21049–21056.

173 C. Shi, K. Chan, J. S. Yoo and J. K. Nørskov, *Org Process Res Dev*, 2016, **20**, 1424–1430.

174 S. Kozuch and S. Shaik, *J Am Chem Soc*, 2006, **128**, 3355–3365.

175 S. Kozuch and S. Shaik, *Acc Chem Res*, 2011, **44**, 101–110.

176 M. R. Singh, J. D. Goodpaster, A. Z. Weber, M. Head-Gordon and A. T. Bell, *Proc Natl Acad Sci*, 2017, **114**, E8812–E8821.

177 S. D. Rihm, J. Akroyd and M. Kraft, *Proceedings of the Combustion Institute*, 2023, **39**, 5647–5655.

178 K. H. Khoo, C. H. Culberson and R. G. Bates, Journal of Solution Chemistry, 1977, **6**, 281–290.

179 S. Kumarampulakkil, A. Naikkath, R. Vinu and R. Srinivasan, *Ionics*, 2025, **31**, 2277–2290.

180 A. S. Varela, W. Ju, A. Bagger, P. Franco, J. Rossmeisl and P. Strasser, *ACS Catal.*, 2019, **9** (8), 7270–7284, DOI: 10.1021/acscatal.9b01405.

No primary research results, software or code have been included and no new data were generated or analysed as part of this review.